Title

The Angiotensin Receptor Blocker Losartan Suppresses Growth of Pulmonary Metastases via AT1R-Independent Inhibition of CCR2 Signaling and Monocyte Recruitment

Journal

The Journal of Immunology, 202(10)

ISSN

0022-1767

Authors

Regan, Daniel P
Coy, Jonathan W
Chahal, Kirti Kandhwal
et al.

Publication Date

2019-05-15

DOI

10.4049/jimmunol.1800619

Peer reviewed

HHS Public Access

Author manuscript

J Immunol. Author manuscript; available in PMC 2020 May 15.

Published in final edited form as:

J Immunol. 2019 May 15; 202(10): 3087–3102. doi:10.4049/jimmunol.1800619.

The Angiotensin Receptor Blocker Losartan Suppresses Growth of Pulmonary Metastases via AT1R-Independent Inhibition of CCR2 Signaling and Monocyte Recruitment

Daniel P. Regan[1,2], **Jonathan W. Coy**[1,3], **Kirti Kandhwal Chahal**[4], **Lyndah Chow**[1,3], **Jade N. Kurihara**[1,3], **Amanda M. Guth**[1,3], **Irina Kufareva**[4], and **Steven W. Dow**[1,3,*]

[1]Flint Animal Cancer Center, College of Veterinary Medicine and Biomedical Sciences, Colorado State University, Fort Collins, CO 80523, USA

[2]Dept. of Microbiology, Immunology, and Pathology, College of Veterinary Medicine and Biomedical Sciences, Colorado State University, Fort Collins, CO 80523, USA

[3]Dept. of Clinical Sciences, College of Veterinary Medicine and Biomedical Sciences, Colorado State University, Fort Collins, CO 80523, USA

[4]Skaggs School of Pharmacy and Pharmaceutical Sciences, University of California San Diego, 9500 Gilman Drive, La Jolla, California 92093, USA

Abstract

Inflammatory monocytes (IMs) have been shown to play key roles in cancer metastasis through promotion of tumor cell extravasation, growth, and angiogenesis. Monocyte recruitment to metastases is mediated primarily via the CCL2-CCR2 chemotactic axis. Thus, disruption of this axis represents an attractive therapeutic target for the treatment of metastatic disease. Losartan, an angiotensin II type 1 receptor (AT1R) antagonist, has been previously shown to have immunomodulatory actions involving monocyte and macrophage activity. However, the exact mechanisms accounting for these effects have not been fully elucidated. Therefore, we investigated the effects of losartan and its primary metabolite on CCL2-mediated monocyte recruitment and CCR2 receptor function using mouse tumor models and in vitro human monocyte cultures. We show here that losartan and its metabolite potently inhibit monocyte recruitment through non-competitive inhibition of CCL2 induced ERK1/2 activation, independent of AT1R receptor activity. Studies in experimental metastasis models demonstrated that losartan treatment significantly reduced the metastatic burden in mice, an effect associated with a significant decrease in $CD11b^{+}/Ly6C^{+}$ recruited monocytes in the lungs. Collectively, these results indicate that losartan can exert anti-metastatic activity by inhibiting CCR2 signaling and suppressing monocyte recruitment, and therefore suggest that losartan (and potentially other ARB drugs) could be repurposed for use in cancer immunotherapy.

[*]**Correspondence:** Dr. Steven Dow, Department of Clinical Sciences, Colorado State University, Ft. Collins, CO 80523, Phone: 970-297-4014, sdow@colostate.edu.

Author Contributions

S.D. and D.R. designed all the experiments. D.R. conducted the experiments and wrote the manuscript. J.C. assisted with image analysis. J.K. and A.G. assisted with animal experiments. I.K. and K.K. designed and conducted the in vitro calcium flux and beta arrestin experiments. S.D. conceptualized and oversaw the experiments, and as senior author assisted with manuscript editing.

The authors have declared that no conflict of interest exists.

Keywords

losartan; inflammatory monocytes; CCL2; CCR2; metastasis

Introduction

Metastasis remains the greatest clinical challenge in cancer treatment, accounting for up to 90% of all cancer-related deaths (1, 2). For example, for breast and colorectal cancer, distant metastases are present in 6 to 21% of patients at the time of diagnosis, respectively (3). Furthermore, although 5-year survival rates experienced by breast and colorectal cancer patients with localized disease are typically excellent, these individuals still have a substantially increased lifetime risk for metastasis, with 30–50% eventually developing disseminated disease (4–6). Thus, the development of new therapies that halt metastatic progression remains a critical hurdle in improving patient outcome.

The tumor microenvironment (TME) is comprised of highly heterogeneous populations of both stromal and immune cells, whose diverse functions collectively promote tumor growth, progression, and eventual metastasis (7, 8). Inflammatory monocytes (IMs) are one component of the TME and have recently been shown to play key roles in the metastatic process (9). For example, CCR2-expressing inflammatory monocytes have been shown to be preferentially recruited early to metastatic sites such as the lung and liver via tumor and stromal cell-mediated production of the monocyte chemoattractant cytokine, CCL2 (10, 11). At sites of metastases, inflammatory monocytes and their derivatives, metastasis-associated macrophages (MAMs), play key roles in promoting metastatic tumor cell extravasation and growth (10, 12–14). In addition, multiple clinical studies have demonstrated a negative prognostic role for increased numbers of inflammatory monocytes and elevated serum CCL2 concentrations in patients with various malignancies, including those of the breast, colon, and pancreas (15–18). Thus, inflammatory monocytes and the CCL2-CCR2 chemotactic axis represent an attractive target for the treatment of cancer metastasis.

Initial clinical trials targeting the CCL2-CCR2 axis in human cancer patients evaluated an anti-human CCL2 monoclonal antibody (Carlumab, CNTO888) and showed that CNTO888 alone or in combination with standard of care therapies was ineffective at slowing tumor progression in patients with various solid tumors (19). However, more recent trials have shown that blockade of the CCL2 receptor, CCR2, has the potential to suppress tumor growth in patients with bone metastases and locally advanced pancreatic cancer, suggesting that inhibition of CCR2 might be a more effective approach in the therapeutic targeting of the CCL2-CCR2 axis (20). While these recent early Phase I/II trials of CCR2 inhibitors are promising, approval is far from certain, as recent data suggests that only 10% of agents entering clinical cancer trials make it to FDA approval (21, 22). Furthermore, the time and cost invested in new drugs is now estimated at a staggering 10 years and $2.6 billion dollars (23). Thus, alternative drug development programs which focus on re-purposing already approved drugs as potential anti-cancer therapies offer greater promise, in terms of reduced cost and time, for getting more effective treatment options to cancer patients (24).

Losartan, a type I angiotensin II receptor (AT1R) blocker (ARB) used in the treatment of hypertension, has been shown to have immunomodulatory and anti-inflammatory properties in models of vascular inflammation and multiple sclerosis (25–27). Interestingly, these anti-inflammatory properties were primarily associated with reduced monocyte and macrophage recruitment to inflammatory lesions and atherosclerotic plaques (25–27). In those studies, losartan blockade of monocyte and macrophage recruitment was attributed to primary inhibition of angiotensin II-AT1R signaling. However, the impact of losartan on CCL2-CCR2 signaling was not investigated. In fact, some molecular modeling studies suggest that losartan and other ARBs have the potential to act as direct CCR2 antagonists (28). Losartan has been investigated for treatment of orthotopic tumors in mice but has not to date been investigated for treatment of tumor metastasis (29, 30). Moreover, the molecular pharmacology underlying losartan's interactions with CCR2, and its potential to act as a CCR2 antagonist, has not been evaluated.

Therefore, in the current work we evaluated the ability of losartan to directly inhibit monocyte migration and recruitment using a combination of *in vitro* and *in vivo* assays of monocyte chemotaxis, monocyte responses to acute inflammation, and monocyte recruitment in early tumor metastasis. Our results demonstrated that both losartan and its primary metabolite (EXP-3174) potently inhibited CCL2-CCR2 dependent recruitment of human and murine monocytes, at clinically relevant concentrations. Furthermore, using G-protein coupled receptor function assays, we characterized the effects of losartan and EXP-3174 on CCL2 ligand binding and post-receptor signal transduction pathways stimulated by CCL2.

Our findings indicated that losartan inhibited CCR2 signaling in a non-competitive manner, in a process independent of effects on AT1R signaling. In experimental metastasis models of breast and colon cancer, losartan treatment significantly slowed metastatic progression, an effect associated with blockade of inflammatory monocyte recruitment and reduction in metastasis-associated macrophages and tumor angiogenesis. Taken together, these studies indicate that losartan (and potentially other ARB drugs) represent a novel class of safe and approved, noncompetitive negative modulators of CCR2 signaling, which could be efficiently repurposed for use in combination therapy for the prevention or treatment of metastatic disease.

Materials and Methods

Experimental animals

6–8-week-old, female BALB/c and ICR mice were purchased from Harlan laboratories (Denver, CO). *CCR2*$^{-/-}$ and *Agtr1*$^{-/-}$ (AT1R$^{-/-}$) mice on the C57BL/6J background and wild-type C57BL/6J mice were purchased from The Jackson Laboratory (Bar Harbor, ME). *CCR2*$^{-/-}$ mice on a BALB/c background were obtained from Dr. Cynthia Ju (University of Colorado, Denver).

Cell lines

4T1-luc, CT26, and CT26-luc cells were generously provided by Dr. Daniel Gustafson (Colorado State University, Fort Collins, CO). THP-1 cells were purchased from the ATCC. CT26-GFP cells were generated by transducing CT26 cells with lentivirus particles expressing GFP under the EF1A promoter (LVP425, GenTarget Inc. San Diego, CA). After 72h cells were treated with G-418 (600 μg/mL; Invivogen, San Diego, CA) to select for successfully transduced cells, and GFP expression was subsequently confirmed by flow cytometry. Cells were maintained in MEM [4T1 and CT26] or RPMI1640 [THP1] media (Gibco, Grand Island, NY USA) supplemented with 10% fetal bovine serum (FBS; Atlas Biologicals, Fort Collins, CO USA), penicillin (100 U/mL), streptomycin (100 μg/mL), L-glutamine (2 mM), and non-essential amino acids (0.1 mM) (All obtained from Gibco). Cells were grown sterilely on standard plastic tissue culture flasks (Cell Treat, Shirley, MA), under standard conditions of 37 °C, 5% CO_2, and humidified air, and were confirmed Mycoplasma-free. *CCR2* expression by THP-1 cells was periodically confirmed by flow cytometry.

Losartan, losartan EXP3174 metabolite, and CCR2 antagonist drugs

50mg losartan potassium tablets (Cozaar) were obtained from the Veterinary Teaching Hospital pharmacy, ground using a mortar and pestle, and dissolved in water and sterile-filtered to obtain a stock concentration of 10mg/mL. Losartan carboxylic acid (EXP3174 metabolite) was purchased as a powder from Santa Cruz Biotechnology (Dallas, TX), and reconstituted in DMSO at 10mg/mL. INCB3284 and RS102895 powder stocks were obtained from Tocris Bioscience (Bristol, UK), and re-constituted in DMSO at 10mg/mL. For all animal experiments, losartan and losartan EXP3174 metabolite drug stocks were diluted in PBS and administered by once daily intra-peritoneal (i.p.) injection of 60mg/kg and 10mg/kg, respectively, in a 100 μL volume.

Experimental lung metastasis models

Wild-type or *CCR2*$^{-/-}$ BALB/c mice were inoculated by I.V. tail vein injection of 1×10^5 4T1-luc cells, 2.5×10^5 CT26-luc cells, or 4×10^5 CT26-GFP cells in 100 μL PBS. Treatment with losartan (60mg/kg, i.p.) was initiated 24h after tumor cell inoculation. For 72h metastasis assays, mice were treated a total of three times (24, 48, and 72h) prior to euthanasia and tissue collection. For long term tumor growth studies, mice were treated daily until study completion. To monitor the development and growth of luciferase-positive pulmonary metastases, bioluminescence imaging was performed thrice weekly using an IVIS100 imager (Perkin-Elmer, Waltham, MA). For imaging, mice were injected i.p. with 100 μL of 30mg/mL luciferin (GoldBio, St. Louis, MO), followed by isoflurane anesthesia and imaging 12 minutes post-luciferin injection (2-minute exposure, medium binning).

In vivo mouse footpad vaccination assay

The cationic liposome-poly I:C adjuvant was prepared in the laboratory as described previously. Using an insulin syringe (BD Biosciences), 50 μl of adjuvant was injected into the right rear footpad of mice while under isoflurane anesthesia. Following injection, mice were immediately treated i.p. with losartan or losartan EXP3174 metabolite (60 mg\kg, or

10mg\kg, respectively), and again 24 hours later. Animals were euthanized ~2 hours following the second drug treatment, and right popliteal lymph nodes (LNs) were harvested and stored in complete media on ice until processing. Right popliteal LNs harvested from naïve, un-injected mice served as controls. LNs were mashed on 40 μM cell-strainers using a 3ml syringe plunger, rinsed with 10ml complete media, centrifuged @1200rpm for 5 min, and re-suspended in FACS buffer for immunostaining and flow cytometry analysis.

Thioglycollate peritonitis model

To induce peritonitis, mice (C57BL/6J wild-type, *CCR2*$^{-/-}$ and *Agtr1*$^{-/-}$) were injected i.p. with 1 mL thioglycollate as described previously (31). Mice were treated with losartan (60mg/kg/day i.p.), beginning ~2h post thioglycollate injection, and continuing once daily until 72h post-injection. Peritoneal leukocytes were collected at 72h by flushing the peritoneal cavity with 10 mL PBS, followed by centrifugation and re-suspension in ACK solution for red cell lysis. Leukocytes were then washed into FACS buffer, and 4×10^5 cells/well were plated in 96 well round-bottom plates for immunostaining and flow cytometry analysis as previously described. Briefly, non-specific binding was blocked by adding normal mouse serum (Jackson Immunoresearch) and un-labeled anti-mouse CD16/32 (eBiosciences) to cells before immunostaining. Cells were then incubated with the following panel of directly labeled rat monoclonal antibodies (eBioscience, San Diego, CA unless otherwise noted) directed against mouse CD11b (clone M1/70), mouse Ly6C (clone AL-21), mouse Ly6G (clone 1A8), mouse CCR2 (clone 475301; R&D Systems), and mouse F4/80 (clone BM8).

In vitro THP-1 and PBMC chemotaxis assays

Peripheral Blood Mononuclear Cells (PBMCs) were isolated from fresh, EDTA-treated human blood by lysing erythrocytes (x2) with ACK buffer solution (150 mM NH_4Cl, 10 mM $KHCO_3$, and 0.1 mM Na_2EDTA). PBMCs were washed into serum-free RPMI (sf-RPMI) and re-suspended at 2×10^6 cells/ml. Cultured THP-1 cells were washed into sf-RPMI and re-suspended at 6×10^6 cells/ml. Drug stocks (losartan, losartan EXP3174 metabolite, or RS102895) were diluted to 2x in sf-RPMI. THP-1 cells or PBMCs were diluted 1:1 in media alone (positive and negative controls) or in media containing 2x drug dilutions. Cells were pre-treated @ 37°C in the incubator for 1 hour prior to plating. The chemotactic stimulus for positive control and drug treated wells consisted of 50 ng/ml recombinant human CCL2 (Peprotech Inc. Rocky Hill, NJ). Negative control wells consisted of sf-RPMI only. THP-1 chemotaxis was conducted in 24-well plates containing 3 μM-pore diameter cell culture inserts (Falcon, Corning, NY). For these assays, 600μl of media +/− *CCL2* was plated in the lower compartment of the plate, while 100 μL (3×10^5) THP-1 cells in media +/− drug were plated in the upper compartment of the cell culture insert. For PBMC migration assays, 96 well chemotaxis plates (Corning, Corning, NY) with an 8 μM pore diameter were used, and 150μl of media +/− CCL2 was plated in the lower compartment of the plate, while 50μl (5×10^4) PBMCs in media +/− drug were plated in the upper compartment of the cell culture insert. Cells were allowed to migrate for 4 h. Following migration, non-migrated cells were removed, wells washed, and membranes (THP-1 migration) or lower compartment wells (PBMCs) were fixed with 4% paraformaldehyde for 10 min on ice, stained with 3% crystal violet (Sigma-Aldrich, St.

Louis, MO USA), rinsed with dH_20, and air-dried overnight. For analysis of THP-1 chemotaxis, membranes were cut from the cell culture inserts, and mounted “migrated-side” up on superfrost plus glass slides using immersion oil. A total of (5) 40x fields per membrane were counted to determine the Mean # of monocytes/40x field for each membrane. For PBMC migration assays, 4×4-tiled 10x magnification overviews of 96 well plates were obtained for each individual well, and total monocytes per/well counted using ImageJ (NIH).

CCL2-induced ERK phosphorylation

Western blot.—THP-1 cells (5×10^5 cells/ well) were plated in 24 well plates and serum starved overnight for ~20–24 hours in the incubator. The following morning, losartan or losartan EXP3174 was added to cultures to achieve the indicated treatment concentrations, and cells were pre-treated for 2 hours prior to CCL2 stimulation. Samples were stimulated with CCL2 (10nM; Peprotech, Rocky Hill, NJ) for 1 min, quickly pelleted, supernatant discarded, and re-suspended in ice-cold lysis buffer [M-PER reagent (ThermoFisher, Waltham, MA) containing 1mM sodium orthovanadate, 100mM PMSF, 2% SDS, and 1x protease inhibitor cocktail (Roche, Basel, Switzerland)] for 10 min on ice. Lysates were then centrifuged at 13,000rpm for 5 min and supernatant removed. For western analysis, (5) μg of THP-1 lysate was mixed 1:1 with 2x Laemelli sample buffer containing 5% 2-Mercaptoethanol (BioRad, Hercules, CA), boiled for 5 minutes, cooled on ice, and then loaded into a Mini-Protean TGX 4–20% pre-cast polyacrylamide gel (BioRad) for electrophoresis (150 V, 45 min). Protein was then transferred to nitrocellulose membranes (95 V, 50 min, at 4 °C), and membranes were blocked for 1 h at RT with 5% BSA in Tris-buffered saline Tween 20 solution (TBST). After washing in TBST, membranes were incubated with the primary antibody (monoclonal rabbit anti-Phospho p44/42 MAPK, clone D13.14.4E, Cell Signaling Technology, Danvers, MA) diluted in 5% BSA-TBST, overnight at 4 °C. The following day membranes were rinsed (x3 with TBST), incubated with the secondary antibody (HRP-linked goat anti-rabbit IgG; ThermoFisher, Waltham, MA) diluted 1: 20,000 in 5% BSA/TBST for 1 h at RT. Lastly, membranes were imaged with chemiluminescent substrate (Clarity Western ECL, BioRad) using a Chemi Doc XES + system (BioRad).

Flow cytometry.—2.5×10^5 THP-1 cells in serum-free RPMI +/− losartan or losartan EXP3174 metabolite at indicated concentrations were incubated for 1h 37°C in microcentrifuge tubes. Following drug pre-treatment, cells were stimulated with 20nM human rCCL2 for 3 min at 37°C. Immediately following stimulation, the reaction was terminated by fixation of cells in an equal volume of 4% paraformaldehyde for 15 min at 37°C. Fixed cells were pelleted, washed twice in FACS buffer, and then permeabilized by re-suspension in 150μL of ice-cold 100% methanol for 15 min. Following permeabilization, cells were washed in FACS (x2), and then stained with monoclonal rabbit anti-human Phospho p44/42 MAPK-AlexaFluor 647 (clone1792G2, Cell Signaling Technology, Danvers, MA) at 1μg/mL diluted in FACS for 30 min at RT. Following primary antibody labeling, cells were washed in FACS (x2), and then analyzed by flow cytometry.

Fluorescence microscopy

Immediately following euthanasia, left lung lobes were dissected and immersion fixed in 1% paraformaldehyde-lysine-periodate fixative (1% paraformaldehyde in 0.2M lysine-HCL, 0.1M anhydrous dibasic sodium phosphate, with 0.21% sodium periodate, pH 7.4) for 24 hours at 4°C. Following fixation, lungs were placed in a 30% w\v sucrose solution for 24 hours at 4°C, prior to embedding and freezing in O.C.T. compound (Tissue Tek). Embedded tissues were sectioned at 5μm for immunostaining. Nonspecific binding was blocked by pre-incubation of sections with 5% donkey serum (Jackson ImmunoResearch, West Grove, PA) in 1% BSA for 30 min at RT. Primary antibody labeling (1:200 anti-GFP, Novus Biologicals; 1:100 anti-F4/80 clone BM8, eBiosciences, and 1:100 anti-Ly6C ab76975) was performed at RT for 1hr in 1% BSA. After removal of the primary antibody, tissues were washed with PBS-T, followed by addition of the following secondary antibodies (diluted 1:200 in PBST) for 30 min at RT: AlexFluor488-conjugated donkey anti-rabbit IgG (GFP), AlexaFluor647-cojugated donkey anti-rat IgG (F4/80), and Cy3-conjugated donkey anti-rat IgG (Ly6C) (Jackson ImmunoResearch). Tissues were counter stained with DAPI, cover-slipped, and visualized using an Olympus IX83 confocal microscope and Hamamatsu digital camera. Figures were assembled using Adobe Photoshop (CC2016).

Fluorescence image capture and image analysis

For quantification of F4/80+ cells within pulmonary micro-metastases and CT26-GFP+ micrometastasis density within lung sections, both single field and whole slide images were captured using standardized exposure times and an Olympus IX83 disc-spinning confocal fluorescence microscope and Hammamatsu Orca R^2 digital camera. All image analysis was performed in a blinded-fashion using ImageJ software (National Institutes of Health), as described below.

To determine the CT26 GFP positive pulmonary micro-metastatic burden, whole slide images were taken with a 4x objective (for 40x total magnification) of both the GFP and DAPI channels. Using the DAPI image, a lower threshold was initially determined using a value corresponding to two standard deviations above the mean fluorescence intensity of slide regions devoid of lung tissue. The accuracy of this threshold value to capture the total lung tissue area was ensured visually by a board-certified pathologist, and subsequently, applied to all images in the data set to generate masks (outlines) that included only the lung tissue area. CT26 GFP positive cells were counted by pixels over a lower threshold limit. This limit was set at a value corresponding to the mean plus 2 standard deviations brightness of control tissue (lung tissue containing no GFP+ tumor cells), again visually ensured for quantification accuracy, and this value universally applied to all images in the data set. The lung tissue area outlines were then over-layered onto masks of CT26-GFP positive cells. CT26-GFP+ tumor cell area was recorded as a percent of total lung tissue area. F4/80+ cell infiltration of micro-metastases was quantified using single field images captured at 20x (200x total) magnification, with all images being centered on GFP+ tumor cell clusters, and all micro-metastases present in the entire lung section capture per animal. For each field, F480+ cells were counted as positive pixels over the lower threshold limit, which was generated in the same manner as described above, and corresponded to a value > two standard deviations above the mean fluorescence intensity of the isotype control, and was

again visually ensured for accuracy by a board-certified pathologist. This threshold limit was then applied universally to all images in the data set.

CCR2 cell surface expression

THP-1 cells, human PBMCs, or mouse bone marrow cells were washed and re-suspended into sf-RPMI at 8×10^5 cells/mL. Drug stocks (10mg/mL) were diluted to either 2x or 4x treatment concentrations for either single agent or combination therapy studies, respectively. 2×10^5 cells in 250uL were plated in 24 well plates and diluted either 1:1 with media alone (control) or 2x drug stocks (single agent treatment), or 1:0.5:0.5 (4x drug stocks, combination treatment studies). Cells +/− drug treatment were then incubated under standard conditions of 37 °C, 5% CO_2, and humidified air for the indicated time periods (1–24hr). Following drug treatment, cells were centrifuged @1800 rpm for 3 minutes, re-suspended in FACS buffer and stained for CCR2 using a monoclonal mouse anti-human CCR2 antibody (clone TG5/CCR2, Biolegend, San Diego, CA). For human PBMCs, cells were also labeled with mouse anti-human CD14 (clone TUK4, Bio-Rad, Hercules, CA). For mouse bone marrow, cells were stained with the following panel of rat monoclonal antibodies directed against: mouse CD11b (clone M1/70), mouse Ly6C (clone AL-21), mouse Ly6G (clone 1A8), and mouse CCR2 (clone 475301; R&D Systems). Data expressed as CCR2 geometric mean fluorescence (gMFI) intensity as % of un-treated controls.

CCR2 mRNA expression in THP-1 cells

Human THP-1 cells were processed and drug treated with losartan, losartan carboxylic acid metabolite (EXP-3174), or a combination of the two drugs at 1 μg/mL for 4 hours or 24 hours as already described in materials and methods. RNA was extracted using Qiagen RNeasy Mini kit (Qiagen Inc., Germantown, MD) according to manufacturer's instructions. The concentration and purity of the RNA was measured using a Nanodrop 1000 (ThermoFisher Scientific, Waltham, MA) with ND-1000 version 3.8.1 software. cDNA was synthesized from 1ug of RNA using QuantiTect® Reverse Transcription kit (Qiagen Inc.) according to manufacturer's instructions. The reaction took place in a MJ Mini Personal Thermal Cycler (Bio-Rad, Hercules, CA). CCR2 expression was measured using RT-PCR with previously published primers (32), normalized to ACTB (β-actin) (33). Concentrations of 100nm for the forward primer and 200nm for the reverse primer were used in the reaction. Master mix containing SYBR Green dye for florescence indication was used (iQ SYBR Green Super Mix, Bio-Rad) in a total reaction volume of 10μL with 20ng of cDNA. Increase of fluorescence to measure amplification was performed by the Mx3000p (Stratagene-Agilent, Santa Clara, CA) and analyzed using the Mx3000p version 2.0 software. 1 cycle of 95°C for 10 min followed by 40 cycles of 95°C for 30 sec and 60°C for 1 min was used. A dissociation curve cycle was also added to confirm that single product was being amplified. Data is expressed as fold change relative to untreated control cells.

CCL2 ligand binding assays

THP-1 cells (2.5×10^5 cells/well) were plated in 96 well plates in chemokine-labeling buffer (RPMI + 20mM HEPES, 10% FBS, 1% L-glutamine, and 1% pen/strep) alone (positive control), or buffer containing either 30nM un-labeled human rCCL2 (cold-competition control), or losartan, losartan EXP3174 metabolite, or INCB3284 at the indicated

concentrations. Human rCCL2-AlexFluor 647 (CAF-2, Almac, Souderton, PA) was then added to all wells to obtain a final concentration of 30nM. Cells were then incubated for 1h @ 37°C, and ligand binding subsequently analyzed by flow cytometry. Data expressed as % inhibition of ligand binding as determined by differences in CCR2 gMFI between untreated and drug treated cells.

Intracellular Ca^{2+} signaling

The FLIPR Calcium 4 assay (Molecular Devices) was performed according to the manufacturer's protocol, with minor modifications. HEK293s cells stably transfected with tetO-CCR2 system (pcDNA6-TR - blasticidin resistant and pACMV-tetO-CCR2 - Geneticin resistant) were maintained under 700 μg/mL Geneticin (Life Technologies) and 5 μg/mL Blasticidin (Fisher Bioreagent) in complete DMEM+10% FBS media. The cells were seeded in poly-D-lysine coated 96 well black/clear-bottom plates (Becton Dickinson Labware) @ 70K cells per well in 100 μL of DMEM + 10% FBS + 2 μg/mL Doxycycline. Twenty-four hours after plating, cell culture medium was replaced with 100 μL of Ca Flux buffer (1X HBSS, 20 mM HEPES, 0.1%BSA) and 10 μL of 24X final concentrations of the test compounds in assay buffer, and 110 μL of FLIPR dye (1X dilution, Becton Dickinson). Following at least 1 hour incubation at 37 °C, the plates were transferred to a FlexStation II-384 plate reader. Wells were injected at t = 18 s with 30 μL of 1.6 μM human recombinant CCL2 (generous gift from Tracy Handel lab, UCSD) (final in-well concentration of 200 nM), and fluorescence was measured for 150 s, reading every 3 s (Ex485/Em525). The difference between maximum (peak) fluorescence and baseline fluorescence was measured in triplicates for each compound concentration and averaged. The experiments were repeated on at least three different days with the data being normalized to the maximum fluorescence observed on the same day for untreated CCR2-expressing cells.

CCR2 β-arrestin recruitment assay

Plasmids—The CCR2b-SmBit and LgBit-β-arrestin1-EE plasmids are generous gift from Asuka Inoue (Graduate School of Pharmaceutical Sciences, Tohoku University, Sendai, Japan). The NanoBiT (34) is a previously published enzyme complementation system derived from the engineered *Oplophorus gracilirostris* luciferase known as NanoLuc (35). The two fragments of NanoBit are the Small Bit (SmBit), which is a variant of the C-terminal fragment of NanoLuc (residues 185-VTGYRLFEEIL-195), and the Large Bit (LgBit), which is a modification of the remaining larger fragment:

> 27-VFTLEDFVGD WEQTAAYNLD QVLEQGGVSS LLQNLAVSVT PIQRIVRSGE NALKIDIHVI
>
> IPYEGLSADQ MAQIEEVFKV VYPVDDHHFK VILPYGTLVI DGVTPNMLNY FGRPYEGIAV-184

Both fragments have been mutated to reduce their mutual binding affinity as described by Dixon et al. (34). CCR2b-SmBit was obtained by fusing the NanoBit SmBiT, with a flexible 15-AA linker (GGSGGGGSGGSSSGG) preceding it, to the C-terminus of human CCR2b in pCAGGS. For this, CCR2b ORF was PCR-amplified using two oligonucleotides:

> 5'-AGAATTGAGCTCCCGGGTACCGCCACCATGCTGTCCACATC-3'

5’-GGACAAAGAAGGAGCCGGGGGATCTGGGGGGGGG-3’ and inserted into a pCAGGS plasmid vector containing the linker and SmBiT by using an NEBuilder HiFi DNA Assembly System (NEB). LgBit-β-arrestin1-EE (36) was obtained by fusing the NanoBit LgBiT to the N-terminus of clathrin-binding-deficient variant of human β-arrestin1 incorporated in pCAGGS vector, with a flexible 16AA linker GGSGGGGSGGSSSGGT between the two. The EE variant contains two mutations (R393E, R395E) in the clathrin/AP-2-binding motif of β-arrestin1, which leads to enhanced retention at the cell plasma membrane and hence an increased receptor recruitment signal (37). The constructs were propagated in E coli using ampicillin (100 μg/mL) as a bacterial selection marker.

Luminescence complementation β-arrestin recruitment assay—HEK293t cells were plated in 6 cm dish. Following a 24 hr incubation at 37°C in 5% CO_2, cells were transiently transfected with CCR2b-SmBit and LgBit-β-arrestin1-EE plasmids (3 μg of each DNA per 6 cm dish). 24 hours post transfection, the cells were lifted with PBS containing 0.2 mM EDTA, centrifuged for 5 min at 400 g, re-suspended in assay buffer (1X HBSS, 5 mM HEPES pH 7.2, 0.05% BSA) and normalized to 1.2×10^6 cell/mL. CTZ-n (Fisher Scientific/#501216836, from 5 mM stock in ethanol) was added to the cell suspension to achieve a final concentration of 10 μM. After that, 80 μL of cell suspension was transferred to 96 well black/clear bottom plate (Falcon/#353219). The plate was incubated at room temperature for approximately 90 min, protected from light. 10 μL of assay buffer or 10 μL of 10x final concentrations of the test compounds (prepared from 10 mM DMSO stocks and diluted in assay buffer) were added to the wells as per plate map, and incubated for 10 min at room temperature, protected from light. A backing tape (PerkinElmer, # 6005199) was applied to the bottom of the plate, after which base luminescence was read for each well using PerkinElmer Victor X Light 2030 (1 sec, no filter). Next, 10 μL of 2 uM CCL2 in assay buffer was added to each well to a final concentration of 200 nM. The cells were incubated at room temperature for 10 min, protected from light, after which the plate was read again for endpoint luminescence. The results were analyzed with GraphPad Prism version 7.0b.

Statistical analysis

All data expressed as means ± SD unless otherwise noted. Statistical significance was determined by a two-tailed, unpaired Student’s *t* test, or One-way ANOVA with Tukey’s post-test for multiple group comparisons. All statistical analyses were performed using Graph Pad Prism software (La Jolla, CA, USA).

Study approval

All animals were housed in microisolator cages in the laboratory animal facility at Colorado State University, and all animal procedures were approved by the Institutional Animal Care and Use Committee at Colorado State University.

Results

Losartan and its primary metabolite (EXP3174) inhibit CCL2-mediated monocyte migration.

The effects of losartan and the primary carboxylic acid metabolite (Los CA; EXP3174) on CCL2-stimulated migration of human monocytic cells (THP-1) were investigated using a trans-well chemotaxis assay (Fig. 1A). Treatment with losartan or EXP3174 significantly inhibited CCL2 stimulated THP-1 migration by up to 90%, compared to untreated cells (*$p<0.05$). Furthermore, the magnitude of monocyte migration inhibition was comparable to that observed for the specific small molecule CCR2 competitive antagonist RS102895, when evaluated at equimolar concentrations, and significant inhibition of CCL2-mediated THP-1 chemotaxis was observed at losartan treatment concentrations as low as 100 ng/mL (Fig. S1 A). Importantly, this blockade of monocyte migration was not secondary to primary cytotoxic effects of losartan or EXP-3174 on THP-1 cells, as treatment concentrations up to 100 μg/mL had no effect on THP-1 growth or survival (Fig. S1 B). Additionally, in contrast to the results of the CCL2 chemotaxis assays, losartan treatment did not significantly block THP-1 migration to the chemokine SDF-1α, a known potent THP-1 chemoattractant and GPCR agonist (38), suggesting that losartan's inhibitory effects were specific to CCL2 mediated chemotaxis (Fig. S1 C). The ability of losartan to block migration of primary human monocytes was also assessed using human peripheral blood mononuclear cells (PBMCs) (Fig. 1B, C). Here again losartan significantly inhibited monocyte migration (by ~50%; *$p<0.04$) at 1 μg/mL, a concentration approximately equal to the maximum plasma levels observed for a single 100 mg oral dose of losartan, a dose routinely used for the treatment of hypertension (39).

Next, the ability of losartan and EXP3174 to inhibit *in vivo* inflammatory monocyte recruitment was assessed using a murine footpad inflammation model, which we have used previously to assess CCL2-CCR2 dependent monocyte recruitment to draining lymph nodes (Fig S1 D) (40). Using this model, we found that administration of losartan or EXP3174 significantly reduced recruitment of inflammatory monocytes to draining LNs by over 75% (**$p<0.01$) (Fig. 1D, E and Fig. S1 E).

In a second approach, the thioglycollate model of aseptic peritonitis was used to evaluate losartan effects on monocyte recruitment to the peritoneal cavity. This model has been previously used for pre-clinical evaluation of other small molecule chemokine receptor antagonists (41, 42). A key feature of this model is that monocyte accumulation in the peritoneal cavity is primarily dependent on CCL2-CCR2 signaling (43, 44). In the present study, we found that losartan treatment (60 mg • kg^{-1} • d^{-1} i.p.) significantly reduced the percentage of $F4/80^{+}/CCR2^{+}$ monocytes accumulating in the peritoneal cavity at 72 hours post-thioglycollate injection, to a level equivalent to that observed in $CCR2^{-/-}$ mice (****$p<0.0001$) (Fig. 1F, J).

Pharmacological characterization of losartan interaction with CCR2

Given the potent monocyte migration inhibitory activity of losartan, additional experiments were conducted to better elucidate the molecular interaction between losartan/EXP-3174 and CCR2. Using the THP-1 cell line (which expresses high levels of CCR2), the effects of

losartan and EXP-3174 metabolite on CCL2 binding and CCL2-induced intracellular Ca^{2+} mobilization were studied. The specific CCR2 orthosteric antagonists BMS681 and INCB3284 were used as positive controls (45, 46). Surprisingly, ligand-binding studies demonstrated that both losartan and EXP-3174 completely failed to block CCL2 binding to CCR2 on THP-1 cells at concentrations ranging from 1 nM to 100 μM (Fig. 2A–C).

In addition, losartan and EXP-3174 had only modest inhibitory effects on CCL2-stimulated cytosolic calcium release, and at equimolar concentrations were significantly less potent than BMS 681 (Fig. 2D). Pre-treatment with losartan and EXP-3174 resulted in a mean maximal inhibition of CCL2-induced calcium responses by 22% and 53%, respectively at doses of 50 μM (**$p<0.01$) (Fig. 2D, E), a concentration equivalent to the maximum plasma concentration (C_{max}) observed in our mouse studies. Significant inhibition of CCL2-induced calcium release was observed with EXP-3174 treatment at concentrations as low as 80nM, although still significantly less potent than BMS 681 (Fig. 2E).

Losartan and EXP-3174 were also evaluated in a second CCR2 functional assay assessing the drugs ability to block CCL2-induced β-arrestin recruitment to CCR2. Consistent with results of the calcium flux assays, significant inhibition of β-arrestin recruitment to CCR2 was again only observed at the high, C_{max} equivalent losartan dose of 50 μM (Fig. 2F–H). Thus, losartan failed to block CCL2 binding to CCR2, and consistent with this observation, only slightly reduced CCL2-induced Ca^{2+} release and β-arrestin recruitment, whereas pure orthosteric CCR2 antagonists were highly active at equivalent concentrations.

Losartan inhibits CCL2-induced ERK1/2 phosphorylation and reduces cell surface CCR2 expression by monocytes

The preceding studies indicated that losartan blockade of monocyte migration was not mediated by competitive inhibition of CCL2 binding to CCR2, nor to any downstream effects on CCL2-mediated cytosolic Ca^{2+} release. Therefore, studies were done next to determine whether losartan inhibited additional targets in the CCL2-CCR2 signaling pathway. Prior studies have demonstrated that CCL2-induced integrin activation and CCR2-dependent monocyte chemotaxis is mediated through the mitogen-activated protein kinase/extracellular signal-regulated kinase (MAPK/ERK) pathway (47–50). Furthermore, these studies also evaluated the specific second messengers involved in CCL2-CCR2 signaling, and demonstrated that CCL2-induced activation of ERK1/2 was in fact independent of changes in cytosolic [Ca^{2+}] or β-arrestin mediated receptor internalization and signaling (47).Thus, the ability of losartan to inhibit CCL2-induced ERK1/2 activation was evaluated in THP-1 cells, using western blot and intracellular flow cytometry assays to assess ERK1/2 phosphorylation (Fig. 3). THP-1 cells were pre-treated with losartan and then stimulated with 20 nM CCL2, a concentration previously reported to induce strong and rapid activation (phosphorylation) of ERK1/2 (47). Both losartan and EXP-3174 significantly inhibited ERK activation in response to CCL2, reducing phospho-ERK1/2 mean fluorescence intensity to levels approximately 30% and 11%, respectively, of those observed in un-treated, CCL2-stimulated positive control cells (Fig. 3A, B). Similarly, ERK1/2 phosphorylation following either acute (Fig. 3C) or chronic/prolonged (Fig. 3D) CCL2 stimulation (as would be expected in a tumor-bearing individual), also revealed that both losartan and EXP-3174

inhibited ERK activation in response to CCL2. For example, losartan and EXP-3174 treatment reduced pERK levels by 29% and 42% following acute CCL2 stimulation (Fig. 3C), respectively, and by 67% and 65%, following prolonged (24h) CCL2 stimulation, respectively (Fig. 3D). A dose-dependent inhibition of ERK1/2 phosphorylation in human CD14+ monocytes by both losartan and EXP-3174, as assessed by flow cytometry, was also observed upon ex-vivo treatment of peripheral blood mononuclear cells (Fig. S2 A, B).

The observed effects of losartan and EXP-3174 on CCL2-induced ERK activation and monocyte chemotaxis could have been mediated by drug-induced receptor down regulation. To address this possibility, the effects of losartan or EXP-3174 pre-treatment on CCR2 expression by THP-1 cells was assessed by flow cytometry. Results of these experiments demonstrated a modest dose and time-dependent reduction in CCR2 expression, occurring early as 4 hours post-treatment (Fig. 3E), with additional receptor downregulation occurring for up to 24 hours post- losartan treatment (Fig. 3F). The CCR2 downregulation effect was additive when losartan and EXP3174 were combined (Fig. 3E, F). In addition, decreased CCR2 cell surface expression was also observed in human peripheral blood CD14+ monocytes (Fig. S2 C) and murine bone-marrow derived $CD11b^{+}/Ly6C^{+}$ monocytes following losartan treatment (Fig. S2 D).

To identify the potential mechanism behind losartan-mediated reduction in surface CCR2 expression, we evaluated the effects of losartan, the EXP-3174 metabolite, or a combination drug treatment on CCR2 mRNA expression in THP-1 cells. These experiments were conducted at the same treatment concentrations and time points performed for the flow cytometric evaluation of CCR2 surface expression shown in Figures 3E and 3F. Results of these experiments demonstrated no effect of losartan treatment on the level of CCR2 gene expression in THP-1 cells (Fig. S2 E and F), ruling out downregulation of CCR2 transcription as a possible mechanism for reduction in cell surface CCR2 protein expression.

Immunofluorescent labeling and flow cytometric evaluation of surface expression of CCR2 or other chemokine receptors is frequently utilized as a surrogate assay to quantify drug or ligand-induced chemokine receptor internalization (51–53). Thus, it was concluded that losartan induced moderate downregulation of CCR2 surface expression on monocytes, independent of an effect on CCR2 gene expression, via a mechanism that most likely involved induction of receptor internalization.

Based on these data, two plausible mechanisms for losartan inhibition of monocyte migration were apparent: 1) Inhibition of CCL2-induced ERK signaling and 2) CCR2 receptor downregulation. We propose that of the two mechanisms, inhibition of ERK signaling was likely the most important pharmacodynamic effect of losartan on monocytes, given that ERK1/2 activation is essential in regulating monocyte migration in response to CCL2. Supporting this notion, ex vivo inhibition of CCL2-induced ERK phosphorylation is a primary pharmacodynamic endpoint for the Pfizer small molecule CCR2 antagonist (PF-04136309) currently being evaluated in a phase II clinical trial (ClinicalTrials.gov NCT 02732938). Thus, our results were most consistent with a model wherein the primary effects of losartan and EXP-3174 were mediated by both direct inhibition of CCR2 signaling

through blockade of ERK activation, as well as a contribution from downregulation of cell surface CCR2 receptor expression.

Losartan inhibition of CCL2-mediated monocyte recruitment and downstream CCR2 signaling are independent of AT1R signaling

Though the preceding studies suggested blockade of CCL2-CCR2-ERK signaling was the primary pharmacodynamic effect of losartan on monocytes, it remained formally possible that this inhibitory activity may have been mediated indirectly via engagement of the angiotensin II type 1 receptor AT1R, the biological target for losartan anti-hypertensive activity. For example, G-protein coupled receptor cross-talk through mechanisms including receptor heterodimerization and allosteric trans-inhibition have been previously described, including examples involving CCR2 (56–59). To address this issue directly, additional studies were performed using $AT1R^{-/-}$ mice.

Importantly, we first noted that lack of AT1R expression had no demonstrable effect on CCL2-mediated monocyte migration, either in vitro or in the thioglycollate peritonitis model (Fig. 4B), thereby eliminating any essential role for AngII-AT1R signaling in these inflammation models. Nonetheless, we observed that ex-vivo treatment of $AT1R^{-/-}$ bone marrow cells with losartan still significantly blocked CCL2-mediated monocyte chemotaxis (Fig. 4A). Moreover, treatment of $AT1R^{-/-}$ mice with losartan (60 mg • kg^{-1} • d^{-1} i.p.) significantly reduced the accumulation of inflammatory monocytes in the peritoneal cavity, to a degree equivalent to $CCR2^{-/-}$ mice (****$p<0.0001$) (Fig. 4B). Furthermore, the inhibitory effects of losartan on CCL2-induced ERK phosphorylation were maintained in $AT1R^{-/-}$ mice, along with the drug's effects on downregulation of cell surface CCR2 expression. For example, treatment with losartan significantly reduced CCL2-mediated ERK1/2 phosphorylation in $Ly6G^{-}\backslash CD11b^{+}\backslash Ly6C^{Hi}$ bone marrow monocytes of $AT1R^{-/-}$ mice by ~50% (Fig. 4C, D). Additionally, once daily losartan treatment significantly reduced cell surface expression of CCR2 on AT1R KO peritoneal macrophages collected 72h post-thioglycollate injection (Fig. 4E, F).

These results suggested therefore that losartan interruption of CCR2 signaling was not mediated by AT1R signaling and also ruled out mechanisms such as AT1R-CCR2 heterodimerization and/or allosteric trans-inhibition. Thus, losartan remained fully active as a monocyte migration blocking agent and inhibitor or ERK1/2 signaling in response to CCL2 even in the absence of the primary losartan intended receptor AT1R (Fig. 4A–F).

Losartan blocks early tumor-mediated inflammatory monocyte recruitment to the lungs and significantly reduces CT26 micrometastases

The preceding studies suggested that losartan may have potential utility as an anti-metastatic agent, given the recognized importance of inflammatory monocytes in the early metastatic events (10). Previous studies have documented losartan-induced suppression of the growth of primary tumors, but to date the effects of losartan or other ARBs on tumor metastasis have not been studied (29, 30, 54). Therefore, studies were done to assess the impact of losartan treatment on metastasis-induced monocyte recruitment to the lungs, using the CT26 lung metastasis model. In this model, tumor metastasis produced a significant increase (~ 4-

fold) in recruitment of $CD11b^{+}/Ly6C^{Hi}$ inflammatory monocytes to the lungs (Fig. 5A, B, & E) within 72 hours of tumor cell injection. In addition, use of $CCR2^{-/-}$ mice in this model demonstrated that the observed monocyte recruitment was entirely dependent on monocyte expression of CCR2 (Fig. 5D & E).

Mice with lung metastases were treated with losartan at a dose of 60 mg • kg^{-1} • d^{-1} i.p. beginning 24 hours after tumor cell injection and were sacrificed at 72 h later. Numbers of infiltrating monocytes were quantitated by flow cytometry and immunofluorescence imaging. Inflammatory monocytes were identified as $Ly6G^{-}/SiglecF^{-}/CD11c^{-}/CD11b^{+}/Ly6C^{Hi}$ cells, and metastasis-associated macrophages (MAMs) were enumerated as $CD11b^{+}/F4/80^{+}$ cells. Losartan treatment significantly reduced the percentages of inflammatory monocytes and MAMs in the lung following tumor injection, by 70% and 36%, respectively, compared to untreated animals. The reduction in numbers of monocytes and macrophages was roughly equivalent to the reduction observed in $CCR2^{-/-}$ mice (Fig. 5C, E, F, & G).

We also noted a striking reduction in the number of CT26-GFP^{+} micro-metastatic colonies in the lungs of losartan-treated mice (Fig. 5H). For example, the area occupied by CT26-GFP micrometastases, quantified as a percentage of the total evaluated lung lobe area, was reduced by 70% in losartan-treated (and by 90% in $CCR2^{-/-}$ mice), compared to untreated control animals (Fig. 5I). These results suggested that losartan treatment and blockade of early tumor-mediated monocyte recruitment to the lung was also associated with decreased tumor cell growth during the early, post-colonization time period.

Losartan mediates sustained blockade of inflammatory monocyte recruitment to suppress CT26 and 4T1 pulmonary metastasis growth

Studies were done next to determine whether losartan treatment could produce sustained inhibition of CCR2 signaling, monocyte recruitment, and suppression of tumor metastasis growth. Luciferase-expressing 4T1 breast or CT26 colon carcinoma cells were injected i.v. and losartan treatment (60 mg • kg^{-1} • d^{-1} i.p.) was initiated 24 hours post-injection, and the lung metastatic burden was monitored 3 times weekly using bioluminescence imaging. Daily treatment with losartan significantly reduced both CT26 and 4T1 pulmonary metastatic burden by 64% and 90%, respectively, as quantified by bioluminescent imaging (CT26: Fig. 6A–C, and 4T1; Fig. 7A–B). In the 4T1 model, losartan-mediated reduction in metastatic tumor burden significantly prolonged overall survival (Fig. 7C, *p=0.04). The reduction in lung metastasis was confirmed via histopathological evaluation of the lungs at euthanasia (Fig. 7D).

Importantly, in both the CT26 and 4T1 models, daily losartan treatment resulted in significant, sustained inhibition of $CD11b^{+}/Ly6C^{Hi}$ monocyte recruitment to the lungs of metastasis-bearing mice, as revealed by flow cytometric analysis. For example, at study termination (day 19 for CT26 mice and day 14 for 4T1 mice) there was a 2-fold reduction in the percentage of lung monocytes in losartan-treated as compared to vehicle (saline)-treated mice (Fig. 6D, E and Fig. 7E, F). Immunofluorescent staining of tissue sections of CT26 and 4T1 pulmonary metastases confirmed the reduction in tumor-infiltrating $F4/80^{+}$ and $CD11b^{+}$ myeloid cells, respectively (Fig. 6D and Fig. 7E).

Monocytes are known to be a rich source of VEGF production, and therefore microvessel density (MVD) in CT26 tumors was assessed via CD31 immunofluorescence imaging. There was a significant 35% reduction in tumor MVD in losartan-treated mice, as compared to untreated tumor-bearing mice (Fig. 6F). Taken together, these results demonstrated that daily losartan treated effectively suppressed breast and colon carcinoma pulmonary colonization and growth, an effect that was associated with a significant reduction in the number of lung monocytes and tumor-associated angiogenesis.

Previous studies have demonstrated that Angiotensin II-AT1R signaling within the tumor stroma can drive tumor-promoting inflammation (55, 56), as well as tumor angiogenesis (57). Thus, it was plausible that the observed anti-tumor effects of losartan in our metastasis models may have been mediated by direct inhibition of AT1R signaling, independent of the observed blockade on monocyte and tumor-macrophage recruitment. To address this question, the experimental metastasis assays and losartan treatments were done in BALB/c CCR2$^{-/-}$ mice. We hypothesized that if the anti-metastatic effects of losartan were mediated in part through AT1R blockade, we should observe enhanced suppression of CT26 metastasis growth in losartan-treated CCR2$^{-/-}$ mice. While metastasis was delayed in CCR2−/− mice (Fig. S3 A, B), losartan treatment did not exert an additive effect in suppressing metastasis in these animals (Fig. S3 A, B), suggesting that the presence of CCR2 was essential and necessary for losartan anti-tumor activity.

In addition, we quantified CCL2 and angiotensin II production by tumor cells in vitro, as well as *in vivo* serum Ang II concentrations in mice with CT26 metastases. Both 4T1 and CT26 cells produced substantially more CCL2 than Ang II (Fig. S3 C), and significantly less Ang II compared to the positive control cell line Lewis Lung Carcinoma(58) (Fig. S3 D). Furthermore, serum Ang II concentrations were not elevated in CT26 metastasis-bearing control (175.7 ± 46.8) or losartan-treated mice (143.4 ± 37.4), compared to mice without tumors (176.1 ± 9.5) (Fig. S3 E, mean ± SEM pg/mL).

Lastly, 72-hour treatment of CT26 or 4T1 cells with a losartan concentration roughly equivalent to overall exposure observed in our *in vivo* pharmacokinetic studies (as determined by AUC0−∞) revealed that there was no direct effect of losartan on tumor cell survival or proliferation (Fig. S3 F). Therefore, these studies excluded Ang II dependent losartan anti-tumor activity, and ruled out direct tumor cell cytotoxic or anti-proliferative action of losartan via AT1R inhibition.

Finally, pharmacokinetic analysis after 14 days of i.p. losartan dosing in mice was performed to address the following two questions: 1) Were plasma losartan concentrations in treated mice equivalent to concentrations used in our in vitro studies, and 2) Were the losartan doses used in our mouse experimental metastasis studies relevant to drug concentrations achieved in humans treated with currently recommended anti-hypertension doses of losartan? With respect to the first question, Fig. S4 A presents the mean plasma concentrations of both losartan and EXP-3174 in mice following a single i.p. dose of 60 mg • kg^{-1} on day 14, and Table 1 in Fig. S4 B summarizes pertinent PK parameters. Indeed, the maximum plasma concentration (C_{max}) and overall exposure (area under the curve, $AUC_{0\text{-}\alpha}$) in these animals was well within the range of the demonstrated effective concentrations in our *in vitro* CCR2

functional assays. For example, the mean maximal plasma concentration of losartan and EXP-3174 in these mice was 24 μg/mL and 23 μg/mL, respectively, which is substantially greater than the 10 μg/mL concentration that demonstrated maximal in vitro inhibition of CCL2-induced ERK1/2 phosphorylation in THP-1 cells in our in vitro studies.

For in vivo dosing, we found that the overall exposure to losartan in treated mice ($AUC_{0-\infty}$ 13 μg • hr • mL^{-1}) was approximately 5–6 times drug concentrations observed in humans administered maximum losartan doses for hypertension or for treatment of Marfan's syndrome (39, 59). While these data suggest dose-escalation studies of losartan in humans may be needed to achieve comparable CCR2 pharmacodynamic (PD) endpoints, it should be noted that a concentration of 1 μg/mL losartan significantly inhibited human CCL2 monocyte migration in vitro, suggesting that the high losartan concentrations achieved in mice may not be required for full activity in humans.

Discussion

Inflammatory monocytes promote multiple steps of the metastatic cascade (9). Multiple studies have demonstrated a critical role for CCL2-CCR2 signaling in regulating monocyte recruitment to metastases (10, 60–62). Clinically, tumor monocyte density, numbers of circulating monocytes or CCL2 concentrations, and tumor CCL2 expression are all well-known as predictors of prognosis of various human malignancies (15–17, 63). Thus, the CCL2-CCR2 axis has become an important potential target for tumor immunotherapy. For example, there are currently two recently completed trials of CCR2 targeted therapies in cancer patients (ClinicalTrials.gov, NCT01015560 and NCT02732938). However, these trials and previous trials targeting CCL2 for cancer immunotherapy have thus far been unsuccessful in achieving their primary study endpoints (19). The reasons for these trial failures are not fully understood, but one explanation has been a failure to fully block CCR2 signaling or to fully neutralize circulating CCL2. Thus, there remains an opportunity for additional novel approaches to more completely block the CCL2-CCR2 signaling axis for cancer immunotherapy.

The ability of the ARB drug losartan to potently block monocyte migration and monocyte mediated inflammatory responses opened the possibility that this drug might be repurposed as a CCR2 antagonist for prevention or early treatment of cancer metastasis, particularly in combination therapy protocols. Our interest in losartan was prompted in part by our frustrating inability to consistently suppress tumor growth using known pure CCR2 antagonist drugs (Dow, S; unpublished data). Prior studies have reported losartan-induced anti-tumor activity, but the effects of losartan on myeloid cell responses were not examined in these studies (29, 30). Therefore, in the present study we investigated alternative explanations for how losartan might inhibit tumor growth and focused on a possible role of blockade of monocyte recruitment through inhibition of CCR2 signaling.

In our studies, *in vitro* chemotaxis assays and *in vivo* models of acute inflammation and experimental pulmonary metastasis both demonstrated that losartan and its primary metabolite (EXP-3174) effectively inhibited CCL2-CCR2 mediated inflammatory monocyte recruitment. Previous studies of losartan and other ARBs in mouse models of atherosclerosis

and immune-mediated encephalomyelitis have demonstrated immunomodulation of monocyte and macrophage activity by ARBs, though in those studies it was concluded that the primary mechanism of action involved inhibition of Ang II-AT1R regulated inflammation. However, our results now suggest that losartan functions primarily as an inhibitor of CCL2-CCR2 mediated inflammation. Indeed, our findings indicate that inhibition of AT1R signaling plays little or no role in the anti-inflammatory effects of losartan treatment. Specifically, our studies in $AT1R^{-/-}$ mice, wherein the suppressive effects of losartan on CCL2-directed monocyte migration, CCR2 cell surface expression, and CCL2-induced ERK phosphorylation remained fully active *both in vitro* and *in vivo*, are consistent with a model in which AT1R signaling plays no role in regulating the effects of losartan on monocyte migration.

Instead, we provide evidence using 3 distinct chemokine receptor function assays that losartan and its primary EXP-3174 metabolite functionally antagonize CCL2-CCR2 signaling independent of any signaling contribution or interaction with its known AT1R target. Our results suggest that the primary pharmacodynamic effect of losartan on monocyte activity occurs at the level of ERK phosphorylation. Highlighting the significance of this finding and substantiating ERK kinase phosphorylation as an important measure of CCR2 target engagement, ex vivo inhibition of CCL2-induced ERK phosphorylation is a secondary outcome measure in a recent clinical trial of the Pfizer small molecule CCR2 antagonist PF-04136309 (ClinicalTrials.gov, NCT02732938). In our studies, losartan inhibition of CCL2-induced ERK phosphorylation occurred independent of blockade of CCL2-ligand binding. Overall, these data are most consistent with a mechanism of non-competitive antagonism of CCR2 signaling. Interestingly, recent crystallography and molecular pharmacology studies of CCR2 have described the presence of a novel, intracellular, allosteric binding site for certain small molecule, non-competitive CCR2 antagonists (46, 64). The observed lack of losartan inhibition of CCL2-ligand binding is however different from the data reported for these novel allosteric antagonists of CCR2 (64).

Thus, the overall results of our CCR2 functional studies and in vivo monocyte recruitment assays in AT1R-deficient mice suggest the presence of an alternative, yet unknown mechanism of losartan functional antagonism of CCR2. While the inhibitory effect of losartan on CCL2-induced ERK phosphorylation could feasibly occur at any point in the ERK signaling cascade downstream of CCR2, the inability of losartan to suppress SDF-1α mediated chemotaxis suggests a more upstream effect of the drug at the level of CCR2 itself. Similar to CCL2, SDF-1α is also a potent chemoattractant of THP-1 cells whose chemotactic effects have been shown to be dependent on ERK signaling. Thus, if losartan non-specifically inhibited ERK signaling at any level downstream of the CCR2 receptor, we would have expected some degree of inhibition of SDF-1 chemotaxis in THP-1 cells, which was not observed in our studies (38, 65, 66). Nevertheless, these data do not fully elucidate the specific activity of losartan on CCR2 signaling, and additional experiments to assess losartan effects on CCR2 activation, specifically CCL2-induced ERK phosphorylation, following site-directed mutagenesis of both the ortho- and allosteric binding pockets of CCR2, are currently underway.

Losartan was also investigated here for its utility as a re-purposed anti-metastatic drug. The effects of losartan treatment on both early and later events in the metastatic cascade were investigated. We found that early tumor colonization of the lung was strongly associated with recruitment of $Ly6C^{Hi}$ monocytes, in a CCR2 dependent manner. Losartan therapy prevented early (72hr) tumor cell colonization, and subsequent monocyte recruitment and MAM accumulation, to a degree similar to that observed in CCR2−/− mice. Longer term daily losartan treatment also suppressed experimental metastasis growth in two different tumor models, and was associated with sustained inhibition of monocyte recruitment and metastasis-associated myeloid cells.

Previous studies in mice have also demonstrated anti-tumor activity by losartan, albeit not in metastasis models, and using doses 3–5 times greater than those used in our studies (29, 30, 54). Recent retrospective analyses of clinical data for patients being treated for hypertension have shown a correlation between the use of losartan, or other ARBs and ACE-inhibitors, and improved outcomes in patients with pancreatic, breast, or lung cancer (67–70). In the pre-clinical rodent studies, losartan's anti-tumor activity was attributed to anti-angiogenic or anti-TGF-β signaling effects, as a result of primary inhibition of Ang II-AT1R signaling. However, it should be noted that many of these previously described losartan effects (e.g. inhibition of tumor angiogenesis, tumor TGF-β production) could also be readily explained by inhibiting monocyte recruitment, as macrophages are known to stimulate both tumor angiogenesis and TGF-β production (71, 72).

Losartan has a long record as a safe anti-hypertensive drug and could therefore be rapidly repurposed as a novel immunotherapeutic drug. One key issue in repurposing losartan is to establish pharmacokinetic equivalency. Therefore, we compared the pharmacokinetics of high-dose losartan administered to mice with previously published losartan PK studies in humans. Direct comparison of losartan C_{max} and $AUC_{0-\infty}$ observed in mice in our study suggested that the 60 mg/kg/day dose used in mice resulted in ~ 6-fold higher drug levels compared to those observed for losartan doses typically used in humans for the treatment of hypertension. However, these drug concentrations may be much higher than those required to effectively block CCR2 signaling. For example, the losartan concentrations that exhibited suppression of chemotaxis and in vitro CCR2 functional assays in our studies were within the range of the C_{max} and $AUC_{0-\infty}$ observed for a single 200 mg oral dose in prior pharmacokinetic studies humans (39). Thus, losartan doses in the range of 2–3 mg • kg^{-1} should achieve these target plasma concentrations. There is precedent for using higher doses of losartan safely, as in the example of Marfan's syndrome patients treated with high-dose losartan, which was safe and well-tolerated (59, 73).

Losartan is an FDA-approved drug with a long safety record and high therapeutic index (74, 75). Our studies demonstrate a unique and previously undescribed mechanism of functional antagonism of CCL2-CCR2 signaling and monocyte recruitment by losartan and its primary EXP-3174 metabolite. These studies also show that daily losartan therapy is effective in suppressing experimental metastasis growth, associated with sustained blockade of inflammatory monocyte mobilization and accumulation of metastasis-associated macrophages. Overall, these findings provide evidence for an important new off-target pharmacological effect of losartan, in addition to its previously reported effects on TGF-β

signaling. Indeed, most or all of the previously reported anti-inflammatory effects of losartan treatment can be explained by monocyte migration inhibition. Thus, further clinical investigations of losartan for modulation of the TME and tumor immunity are warranted.

Supplementary Material

Refer to Web version on PubMed Central for supplementary material.

Acknowledgements

We thank Dr. Tracy Handel (University of California-San Diego) for valuable input regarding CCR2 functional assays. Additionally, we'd like to thank Dr. Daniel Gustafson, Dr. Ryan Hansen, and Paul Lunghofer (Flint Animal Cancer Center, Colorado State University) for conducting the losartan pharmacokinetic studies in mice. The authors also thank Asuka Inoue (Graduate School of Pharmaceutical Sciences, Tohoku University, Sendai, Japan) for providing the CCR2b-SmBit and LgBit-β-arrestin1-EE plasmids.

The work for this project was supported by the Shipley Foundation (SWD), as well as NIH grants T32OD010437 (DPR) and K01OD022982 (DPR), and R01AI118985, R01GM117424, R35HL135737 and R01NS102432 (all to IK).

References

1. Mehlen P, and Puisieux A. 2006 Metastasis: a question of life or death. Nat Rev Cancer 6: 449–458. [PubMed: 16723991]
2. Monteiro J, and Fodde R. 2010 Cancer stemness and metastasis: therapeutic consequences and perspectives. Eur J Cancer 46: 1198–1203. [PubMed: 20303259]
3. Howlader N,NA, Krapcho M, Miller D, Bishop K, Altekruse SF, Kosary CL, Yu M, Ruhl J, Tatalovich Z, Mariotto A, Lewis DR, Chen HS, Feuer EJ, Cronin KA (eds). SEER Cancer Statistics Review, 1975–2013, National Cancer Institute Bethesda, MD, http://seer.cancer.gov/csr/1975_2013/, based on November 2015 SEER data submission, posted to the SEER web site, 4 2016.
4. Weigelt B, Peterse JL, and van 't Veer LJ. 2005 Breast cancer metastasis: markers and models. Nat Rev Cancer 5: 591–602. [PubMed: 16056258]
5. O'Shaughnessy J 2005 Extending survival with chemotherapy in metastatic breast cancer. The oncologist 10 Suppl 3: 20–29. [PubMed: 16368868]
6. Van Cutsem E, and Oliveira J. 2009 Advanced colorectal cancer: ESMO clinical recommendations for diagnosis, treatment and follow-up. Annals of oncology : official journal of the European Society for Medical Oncology 20 Suppl 4: 61–63. [PubMed: 19454465]
7. Steeg PS 2016 Targeting metastasis. Nat Rev Cancer 16: 201–218. [PubMed: 27009393]
8. Hanahan D, and Weinberg RA. 2011 Hallmarks of cancer: the next generation. Cell 144: 646–674. [PubMed: 21376230]
9. Kitamura T, Qian BZ, and Pollard JW. 2015 Immune cell promotion of metastasis. Nat Rev Immunol 15: 73–86. [PubMed: 25614318]
10. Qian BZ, Li J, Zhang H, Kitamura T, Zhang J, Campion LR, Kaiser EA, Snyder LA, and Pollard JW. 2011 CCL2 recruits inflammatory monocytes to facilitate breast-tumour metastasis. Nature 475: 222–225. [PubMed: 21654748]
11. Piao C, Cai L, Qiu S, Jia L, Song W, and Du J. 2015 Complement 5a Enhances Hepatic Metastases of Colon Cancer via Monocyte Chemoattractant Protein-1-mediated Inflammatory Cell Infiltration. The Journal of biological chemistry 290: 10667–10676. [PubMed: 25739439]
12. Qian BZ, Zhang H, Li J, He T, Yeo EJ, Soong DY, Carragher NO, Munro A, Chang A, Bresnick AR, Lang RA, and Pollard JW. 2015 FLT1 signaling in metastasis-associated macrophages activates an inflammatory signature that promotes breast cancer metastasis. J Exp Med 212: 1433–1448. [PubMed: 26261265]

13. Chen Q, Zhang XH, and Massague J. 2011 Macrophage binding to receptor VCAM-1 transmits survival signals in breast cancer cells that invade the lungs. Cancer Cell 20: 538–549. [PubMed: 22014578]

14. Mazzieri R, Pucci F, Moi D, Zonari E, Ranghetti A, Berti A, Politi LS, Gentner B, Brown JL, Naldini L, and De Palma M. 2011 Targeting the ANG2/TIE2 axis inhibits tumor growth and metastasis by impairing angiogenesis and disabling rebounds of proangiogenic myeloid cells. Cancer Cell 19: 512–526. [PubMed: 21481792]

15. Sanford DE, Belt BA, Panni RZ, Mayer A, Deshpande AD, Carpenter D, Mitchem JB, Plambeck-Suess SM, Worley LA, Goetz BD, Wang-Gillam A, Eberlein TJ, Denardo DG, Goedegebuure SP, and Linehan DC. 2013 Inflammatory monocyte mobilization decreases patient survival in pancreatic cancer: a role for targeting the CCL2/CCR2 axis. Clin Cancer Res 19: 3404–3415. [PubMed: 23653148]

16. Sasaki A, Kai S, Endo Y, Iwaki K, Uchida H, Tominaga M, Okunaga R, Shibata K, Ohta M, and Kitano S. 2007 Prognostic value of preoperative peripheral blood monocyte count in patients with colorectal liver metastasis after liver resection. Journal of gastrointestinal surgery : official journal of the Society for Surgery of the Alimentary Tract 11: 596–602. [PubMed: 17468918]

17. Ni XJ, Zhang XL, Ou-Yang QW, Qian GW, Wang L, Chen S, Jiang YZ, Zuo WJ, Wu J, Hu X, and Shao ZM. 2014 An elevated peripheral blood lymphocyte-to-monocyte ratio predicts favorable response and prognosis in locally advanced breast cancer following neoadjuvant chemotherapy. PLoS One 9: e111886. [PubMed: 25372468]

18. Svensson S, Abrahamsson A, Rodriguez GV, Olsson AK, Jensen L, Cao Y, and Dabrosin C. 2015 CCL2 and CCL5 Are Novel Therapeutic Targets for Estrogen-Dependent Breast Cancer. Clin Cancer Res 21: 3794–3805. [PubMed: 25901081]

19. Sandhu SK, Papadopoulos K, Fong PC, Patnaik A, Messiou C, Olmos D, Wang G, Tromp BJ, Puchalski TA, Balkwill F, Berns B, Seetharam S, de Bono JS, and Tolcher AW. 2013 A first-in-human, first-in-class, phase I study of carlumab (CNTO 888), a human monoclonal antibody against CC-chemokine ligand 2 in patients with solid tumors. Cancer chemotherapy and pharmacology 71: 1041–1050. [PubMed: 23385782]

20. Nywening TM, Wang-Gillam A, Sanford DE, Belt BA, Panni RZ, Cusworth BM, Toriola AT, Nieman RK, Worley LA, Yano M, Fowler KJ, Lockhart AC, Suresh R, Tan BR, Lim KH, Fields RC, Strasberg SM, Hawkins WG, DeNardo DG, Goedegebuure SP, and Linehan DC. 2016 Targeting tumour-associated macrophages with CCR2 inhibition in combination with FOLFIRINOX in patients with borderline resectable and locally advanced pancreatic cancer: a single-centre, open-label, dose-finding, non-randomised, phase 1b trial. The Lancet. Oncology 17: 651–662. [PubMed: 27055731]

21. DiMasi JA, and Grabowski HG. 2007 Economics of new oncology drug development. J Clin Oncol 25: 209–216. [PubMed: 17210942]

22. Kola I, and Landis J. 2004 Can the pharmaceutical industry reduce attrition rates? Nature reviews. Drug discovery 3: 711–715. [PubMed: 15286737]

23. Mullard A 2014 New drugs cost US[dollar]2.6 billion to develop. Nature reviews. Drug discovery 13: 877–877.

24. Bertolini F, Sukhatme VP, and Bouche G. 2015 Drug repurposing in oncology--patient and health systems opportunities. Nature reviews. Clinical oncology 12: 732–742.

25. Stegbauer J, Lee DH, Seubert S, Ellrichmann G, Manzel A, Kvakan H, Muller DN, Gaupp S, Rump LC, Gold R, and Linker RA. 2009 Role of the renin-angiotensin system in autoimmune inflammation of the central nervous system. Proc Natl Acad Sci U S A 106: 14942–14947. [PubMed: 19706425]

26. Yang J, Sun Y, Dong M, Yang X, Meng X, Niu R, Guan J, Zhang Y, and Zhang C. 2015 Comparison of angiotensin-(1–7), losartan and their combination on atherosclerotic plaque formation in apolipoprotein E knockout mice. Atherosclerosis 240: 544–549. [PubMed: 25957120]

27. Dai Q, Xu M, Yao M, and Sun B. 2007 Angiotensin AT1 receptor antagonists exert anti-inflammatory effects in spontaneously hypertensive rats. British journal of pharmacology 152: 1042–1048. [PubMed: 17922026]

28. Marshall TG, Lee RE, and Marshall FE. 2006 Common angiotensin receptor blockers may directly modulate the immune system via VDR, PPAR and CCR2b. Theoretical biology & medical modelling 3: 1. [PubMed: 16403216]
29. Arnold SA, Rivera LB, Carbon JG, Toombs JE, Chang CL, Bradshaw AD, and Brekken RA. 2012 Losartan slows pancreatic tumor progression and extends survival of SPARC-null mice by abrogating aberrant TGFbeta activation. PLoS One 7: e31384. [PubMed: 22348081]
30. Otake AH, Mattar AL, Freitas HC, Machado CM, Nonogaki S, Fujihara CK, Zatz R, and Chammas R. 2010 Inhibition of angiotensin II receptor 1 limits tumor-associated angiogenesis and attenuates growth of murine melanoma. Cancer chemotherapy and pharmacology 66: 79–87. [PubMed: 19771429]
31. Boring L, Gosling J, Chensue SW, Kunkel SL, Farese RV Jr., Broxmeyer HE, and Charo IF. 1997 Impaired monocyte migration and reduced type 1 (Th1) cytokine responses in C-C chemokine receptor 2 knockout mice. J Clin Invest 100: 2552–2561. [PubMed: 9366570]
32. Sasaki Y, Dehnad A, Fish S, Sato A, Jiang J, Tian J, Schroder K, Brandes R, and Torok NJ. 2017 NOX4 Regulates CCR2 and CCL2 mRNA Stability in Alcoholic Liver Disease. Scientific reports 7: 46144. [PubMed: 28383062]
33. Maess MB, Sendelbach S, and Lorkowski S. 2010 Selection of reliable reference genes during THP-1 monocyte differentiation into macrophages. BMC molecular biology 11: 90. [PubMed: 21122122]
34. Dixon AS, Schwinn MK, Hall MP, Zimmerman K, Otto P, Lubben TH, Butler BL, Binkowski BF, Machleidt T, Kirkland TA, Wood MG, Eggers CT, Encell LP, and Wood KV. 2016 NanoLuc Complementation Reporter Optimized for Accurate Measurement of Protein Interactions in Cells. ACS chemical biology 11: 400–408. [PubMed: 26569370]
35. England CG, Ehlerding EB, and Cai W. 2016 NanoLuc: A Small Luciferase Is Brightening Up the Field of Bioluminescence. Bioconjugate chemistry 27: 1175–1187. [PubMed: 27045664]
36. Shihoya W, Izume T, Inoue A, Yamashita K, Kadji FMN, Hirata K, Aoki J, Nishizawa T, and Nureki O. 2018 Crystal structures of human ETB receptor provide mechanistic insight into receptor activation and partial activation. Nature communications 9: 4711.
37. Kim YM, and Benovic JL. 2002 Differential roles of arrestin-2 interaction with clathrin and adaptor protein 2 in G protein-coupled receptor trafficking. The Journal of biological chemistry 277: 30760–30768. [PubMed: 12070169]
38. Tian Y, New DC, Yung LY, Allen RA, Slocombe PM, Twomey BM, Lee MMK, and Wong YH. 2004 Differential chemokine activation of CC chemokine receptor 1-regulated pathways: ligand selective activation of Galpha 14-coupled pathways. European journal of immunology 34: 785–795. [PubMed: 14991608]
39. Ohtawa M, Takayama F, Saitoh K, Yoshinaga T, and Nakashima M. 1993 Pharmacokinetics and biochemical efficacy after single and multiple oral administration of losartan, an orally active nonpeptide angiotensin II receptor antagonist, in humans. British journal of clinical pharmacology 35: 290–297. [PubMed: 8471405]
40. Mitchell LA, Henderson AJ, and Dow SW. 2012 Suppression of vaccine immunity by inflammatory monocytes. J Immunol 189: 5612–5621. [PubMed: 23136203]
41. Lefebvre E, Moyle G, Reshef R, Richman LP, Thompson M, Hong F, Chou HL, Hashiguchi T, Plato C, Poulin D, Richards T, Yoneyama H, Jenkins H, Wolfgang G, and Friedman SL. 2016 Antifibrotic Effects of the Dual CCR2/CCR5 Antagonist Cenicriviroc in Animal Models of Liver and Kidney Fibrosis. PLoS One 11: e0158156. [PubMed: 27347680]
42. Laborde E, Macsata RW, Meng F, Peterson BT, Robinson L, Schow SR, Simon RJ, Xu H, Baba K, Inagaki H, Ishiwata Y, Jomori T, Matsumoto Y, Miyachi A, Nakamura T, Okamoto M, Handel TM, and Bernard CC. 2011 Discovery, optimization, and pharmacological characterization of novel heteroaroylphenylureas antagonists of C-C chemokine ligand 2 function. Journal of medicinal chemistry 54: 1667–1681. [PubMed: 21341682]
43. Takahashi M, Galligan C, Tessarollo L, and Yoshimura T. 2009 Monocyte chemoattractant protein-1 (MCP-1), not MCP-3, is the primary chemokine required for monocyte recruitment in mouse peritonitis induced with thioglycollate or zymosan A. J Immunol 183: 3463–3471. [PubMed: 19641140]

44. Tsou CL, Peters W, Si Y, Slaymaker S, Aslanian AM, Weisberg SP, Mack M, and Charo IF. 2007 Critical roles for CCR2 and MCP-3 in monocyte mobilization from bone marrow and recruitment to inflammatory sites. J Clin Invest 117: 902–909. [PubMed: 17364026]
45. Xue CB, Feng H, Cao G, Huang T, Glenn J, Anand R, Meloni D, Zhang K, Kong L, Wang A, Zhang Y, Zheng C, Xia M, Chen L, Tanaka H, Han Q, Robinson DJ, Modi D, Storace L, Shao L, Sharief V, Li M, Galya LG, Covington M, Scherle P, Diamond S, Emm T, Yeleswaram S, Contel N, Vaddi K, Newton R, Hollis G, Friedman S, and Metcalf B. 2011 Discovery of INCB3284, a Potent, Selective, and Orally Bioavailable hCCR2 Antagonist. ACS medicinal chemistry letters 2: 450–454. [PubMed: 24900329]
46. Zheng Y, Qin L, Zacarias NV, de Vries H, Han GW, Gustavsson M, Dabros M, Zhao C, Cherney RJ, Carter P, Stamos D, Abagyan R, Cherezov V, Stevens RC, AP IJ, Heitman LH, Tebben A, Kufareva I, and Handel TM. 2016 Structure of CC chemokine receptor 2 with orthosteric and allosteric antagonists. Nature 540: 458–461. [PubMed: 27926736]
47. Jimenez-Sainz MC, Fast B, Mayor F Jr., and Aragay AM. 2003 Signaling pathways for monocyte chemoattractant protein 1-mediated extracellular signal-regulated kinase activation. Molecular pharmacology 64: 773–782. [PubMed: 12920215]
48. Ashida N, Arai H, Yamasaki M, and Kita T. 2001 Distinct signaling pathways for MCP-1-dependent integrin activation and chemotaxis. The Journal of biological chemistry 276: 16555–16560. [PubMed: 11278464]
49. Dubois PM, Palmer D, Webb ML, Ledbetter JA, and Shapiro RA. 1996 Early signal transduction by the receptor to the chemokine monocyte chemotactic protein-1 in a murine T cell hybrid. J Immunol 156: 1356–1361. [PubMed: 8568234]
50. Yen H, Zhang Y, Penfold S, and Rollins BJ. 1997 MCP-1-mediated chemotaxis requires activation of non-overlapping signal transduction pathways. J Leukoc Biol 61: 529–532. [PubMed: 9103241]
51. Ajram L, Begg M, Slack R, Cryan J, Hall D, Hodgson S, Ford A, Barnes A, Swieboda D, Mousnier A, and Solari R. 2014 Internalization of the chemokine receptor CCR4 can be evoked by orthosteric and allosteric receptor antagonists. European journal of pharmacology 729: 75–85. [PubMed: 24534492]
52. Berchiche YA, Gravel S, Pelletier ME, St-Onge G, and Heveker N. 2011 Different effects of the different natural CC chemokine receptor 2b ligands on beta-arrestin recruitment, Galphai signaling, and receptor internalization. Molecular pharmacology 79: 488–498. [PubMed: 21088225]
53. Mack M, Cihak J, Simonis C, Luckow B, Proudfoot AE, Plachy J, Bruhl H, Frink M, Anders HJ, Vielhauer V, Pfirstinger J, Stangassinger M, and Schlondorff D. 2001 Expression and characterization of the chemokine receptors CCR2 and CCR5 in mice. J Immunol 166: 4697–4704. [PubMed: 11254730]
54. Noguchi R, Yoshiji H, Ikenaka Y, Namisaki T, Kitade M, Kaji K, Yoshii J, Yanase K, Yamazaki M, Tsujimoto T, Kawaratani H, and Fukui H. 2009 Synergistic inhibitory effect of gemcitabine and angiotensin type-1 receptor blocker, losartan, on murine pancreatic tumor growth via anti-angiogenic activities. Oncology reports 22: 355–360. [PubMed: 19578777]
55. Suzuki Y, Ruiz-Ortega M, Lorenzo O, Ruperez M, Esteban V, and Egido J. 2003 Inflammation and angiotensin II. The international journal of biochemistry & cell biology 35: 881–900. [PubMed: 12676174]
56. Chehl N, Gong Q, Chipitsyna G, Aziz T, Yeo CJ, and Arafat HA. 2009 Angiotensin II regulates the expression of monocyte chemoattractant protein-1 in pancreatic cancer cells. Journal of gastrointestinal surgery : official journal of the Society for Surgery of the Alimentary Tract 13: 2189–2200. [PubMed: 19816747]
57. Fujita M, Hayashi I, Yamashina S, Fukamizu A, Itoman M, and Majima M. 2005 Angiotensin type 1a receptor signaling-dependent induction of vascular endothelial growth factor in stroma is relevant to tumor-associated angiogenesis and tumor growth. Carcinogenesis 26: 271–279. [PubMed: 15637093]
58. Fan L, Feng Y, Wan HY, Ni L, Qian YR, Guo Y, Xiang Y, and Li QY. 2014 Hypoxia induces dysregulation of local renin-angiotensin system in mouse Lewis lung carcinoma cells. Genetics and molecular research : GMR 13: 10562–10573. [PubMed: 25511041]

59. Falvella FS, Marelli S, Cheli S, Montanelli S, Viecca F, Salvi L, Ferrara A, Clementi E, Trifiro G, and Pini A. 2016 Pharmacogenetic approach to losartan in Marfan patients: a starting point to improve dosing regimen? Drug metabolism and personalized therapy 31: 157–163. [PubMed: 27474842]
60. Zhao L, Lim SY, Gordon-Weeks AN, Tapmeier TT, Im JH, Cao Y, Beech J, Allen D, Smart S, and Muschel RJ. 2013 Recruitment of a myeloid cell subset (CD11b/Gr1 mid) via CCL2/CCR2 promotes the development of colorectal cancer liver metastasis. Hepatology (Baltimore, Md.) 57: 829–839.
61. van Deventer HW, Palmieri DA, Wu QP, McCook EC, and Serody JS. 2013 Circulating fibrocytes prepare the lung for cancer metastasis by recruiting Ly-6C+ monocytes via CCL2. J Immunol 190: 4861–4867. [PubMed: 23536638]
62. Hoos A, Protsyuk D, and Borsig L. 2014 Metastatic growth progression caused by PSGL-1-mediated recruitment of monocytes to metastatic sites. Cancer Res 74: 695–704. [PubMed: 24322980]
63. Izumi K, Mizokami A, Lin HP, Ho HM, Iwamoto H, Maolake A, Natsagdorj A, Kitagawa Y, Kadono Y, Miyamoto H, Huang CK, Namiki M, and Lin WJ. 2016 Serum chemokine (CC motif) ligand 2 level as a diagnostic, predictive, and prognostic biomarker for prostate cancer. Oncotarget 7: 8389–8398. [PubMed: 26701731]
64. Zweemer AJ, Bunnik J, Veenhuizen M, Miraglia F, Lenselink EB, Vilums M, de Vries H, Gibert A, Thiele S, Rosenkilde MM, AP IJ, and Heitman LH. 2014 Discovery and mapping of an intracellular antagonist binding site at the chemokine receptor CCR2. Molecular pharmacology 86: 358–368. [PubMed: 25024169]
65. Tripathi A, Davis JD, Staren DM, Volkman BF, and Majetschak M. 2014 CXC chemokine receptor 4 signaling upon co-activation with stromal cell-derived factor-1alpha and ubiquitin. Cytokine 65: 121–125. [PubMed: 24373940]
66. Arai A, Aoki M, Weihua Y, Jin A, and Miura O. 2006 CrkL plays a role in SDF-1-induced activation of the Raf-1/MEK/Erk pathway through Ras and Rac to mediate chemotactic signaling in hematopoietic cells. Cellular signalling 18: 2162–2171. [PubMed: 16781119]
67. Chae YK, Valsecchi ME, Kim J, Bianchi AL, Khemasuwan D, Desai A, and Tester W. 2011 Reduced risk of breast cancer recurrence in patients using ACE inhibitors, ARBs, and/or statins. Cancer investigation 29: 585–593. [PubMed: 21936625]
68. Miao L, Chen W, Zhou L, Wan H, Gao B, and Feng Y. 2016 Impact of Angiotensin I-converting Enzyme Inhibitors and Angiotensin II Type-1 Receptor Blockers on Survival of Patients with NSCLC. Scientific reports 6: 21359. [PubMed: 26883083]
69. Nakai Y, Isayama H, Ijichi H, Sasaki T, Sasahira N, Hirano K, Kogure H, Kawakubo K, Yagioka H, Yashima Y, Mizuno S, Yamamoto K, Arizumi T, Togawa O, Matsubara S, Tsujino T, Tateishi K, Tada M, Omata M, and Koike K. 2010 Inhibition of renin-angiotensin system affects prognosis of advanced pancreatic cancer receiving gemcitabine. British journal of cancer 103: 1644–1648. [PubMed: 20978506]
70. Rhodes DR, Ateeq B, Cao Q, Tomlins SA, Mehra R, Laxman B, Kalyana-Sundaram S, Lonigro RJ, Helgeson BE, Bhojani MS, Rehemtulla A, Kleer CG, Hayes DF, Lucas PC, Varambally S, and Chinnaiyan AM. 2009 AGTR1 overexpression defines a subset of breast cancer and confers sensitivity to losartan, an AGTR1 antagonist. Proc Natl Acad Sci U S A 106: 10284–10289. [PubMed: 19487683]
71. Dalton HJ, Armaiz-Pena GN, Gonzalez-Villasana V, Lopez-Berestein G, Bar-Eli M, and Sood AK. 2014 Monocyte subpopulations in angiogenesis. Cancer Res 74: 1287–1293. [PubMed: 24556724]
72. Solinas G, Germano G, Mantovani A, and Allavena P. 2009 Tumor-associated macrophages (TAM) as major players of the cancer-related inflammation. J Leukoc Biol 86: 1065–1073. [PubMed: 19741157]
73. Brooke BS, Habashi JP, Judge DP, Patel N, Loeys B, and Dietz HC 3rd. 2008 Angiotensin II blockade and aortic-root dilation in Marfan's syndrome. N Engl J Med 358: 2787–2795. [PubMed: 18579813]
74. Burnier M, Waeber B, and Brunner HR. 1995 Clinical pharmacology of the angiotensin II receptor antagonist losartan potassium in healthy subjects. Journal of hypertension. Supplement : official journal of the International Society of Hypertension 13: S23–28. [PubMed: 18800452]

75. McIntyre M, Caffe SE, Michalak RA, and Reid JL. 1997 Losartan, an orally active angiotensin (AT1) receptor antagonist: a review of its efficacy and safety in essential hypertension. Pharmacology & therapeutics 74: 181–194. [PubMed: 9336021]

Key Points

Losartan blocks CCL2-CCR2 monocyte recruitment to suppress lung metastasis growth.

Losartan functionally antagonizes CCL2-CCR2 ERK activation, independent of its AT1R target.

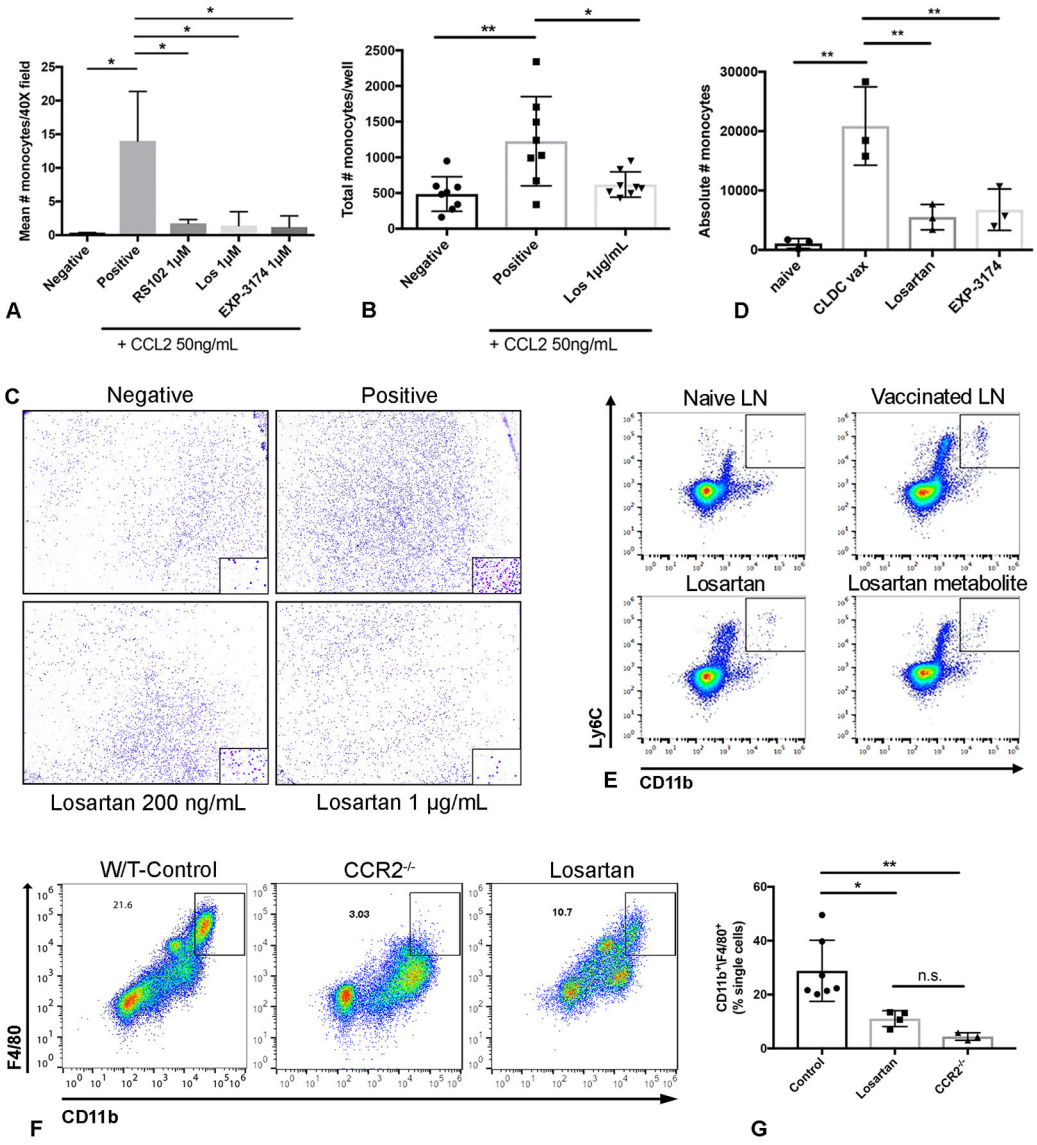

Figure 1.

Losartan and its primary metabolite EXP3174 inhibit *CCL2-CCR2* mediated monocyte migration *in vitro* and *in vivo* at pharmacologically relevant concentrations. **(A)** Quantitative bar graph of in vitro trans-well migration assays assessing the ability of losartan (Los) and its metabolite EXP3174 (losartan carboxylic acid, Los CA) to inhibit *CCL2*-directed THP-1 monocyte migration as compared to the specific small molecule *CCR2* antagonist RS102895 (RS102). *p < 0.05, one-way ANOVA, *n* = means of 3 independent experiments performed in triplicate. **(B)** Quantitative bar graph demonstrating the effects of clinically relevant concentrations of losartan on in vitro *CCL2*-mediated human PBMC migration. **p < 0.01, *p < 0.05, one-way ANOVA, *n* = 8 replicates pooled from two independent experiments. **(C)** Representative whole well images (10x) and higher magnification (40x; inset) of human PBMC migration assays quantified in **B**. **(D)** Quantification of the absolute numbers of IMs, as detected by flow cytometry, in vaccine-draining popliteal LNs of groups of mice shown in

E. **p < 0.01, one-way ANOVA, *n* =3 per group, representative of two independent experiments. **(E)** Representative flow plots of the data shown in **D** demonstrating the ability of losartan and its metabolite to inhibit the recruitment of *Ly6G^{-}/CD11b^{+}/Gr1(Ly6C)^{Hi}* inflammatory monocytes (IMs) to vaccine-draining popliteal lymph nodes (LNs) of mice. This recruitment is almost entirely dependent on the CCL2-CCR2 axis (Fig. S1). **(F)** Representative dot plots of *CD11b^{+}/F4/80^{+}* monocytes in peritoneal lavage fluid collected 72h post i.p. injection of thioglycollate in wild-type C57BL/6J mice *(top left)*, CCR2$^{-/-}$ mice *(top right)*, or wild-type mice treated with losartan 60mg/kg/day *(bottom left)*. **(G)** Graph depicting the flow-cytometric quantification of CD11b^{+}/F4/80^{+} peritoneal monocytes for the groups of mice in **F**. **p < 0.01, *p < 0.05, n.s. p > 0.05, one-way ANOVA, *n* = 3–7 per group, pooled from two independent experiments. All error bars, SD.

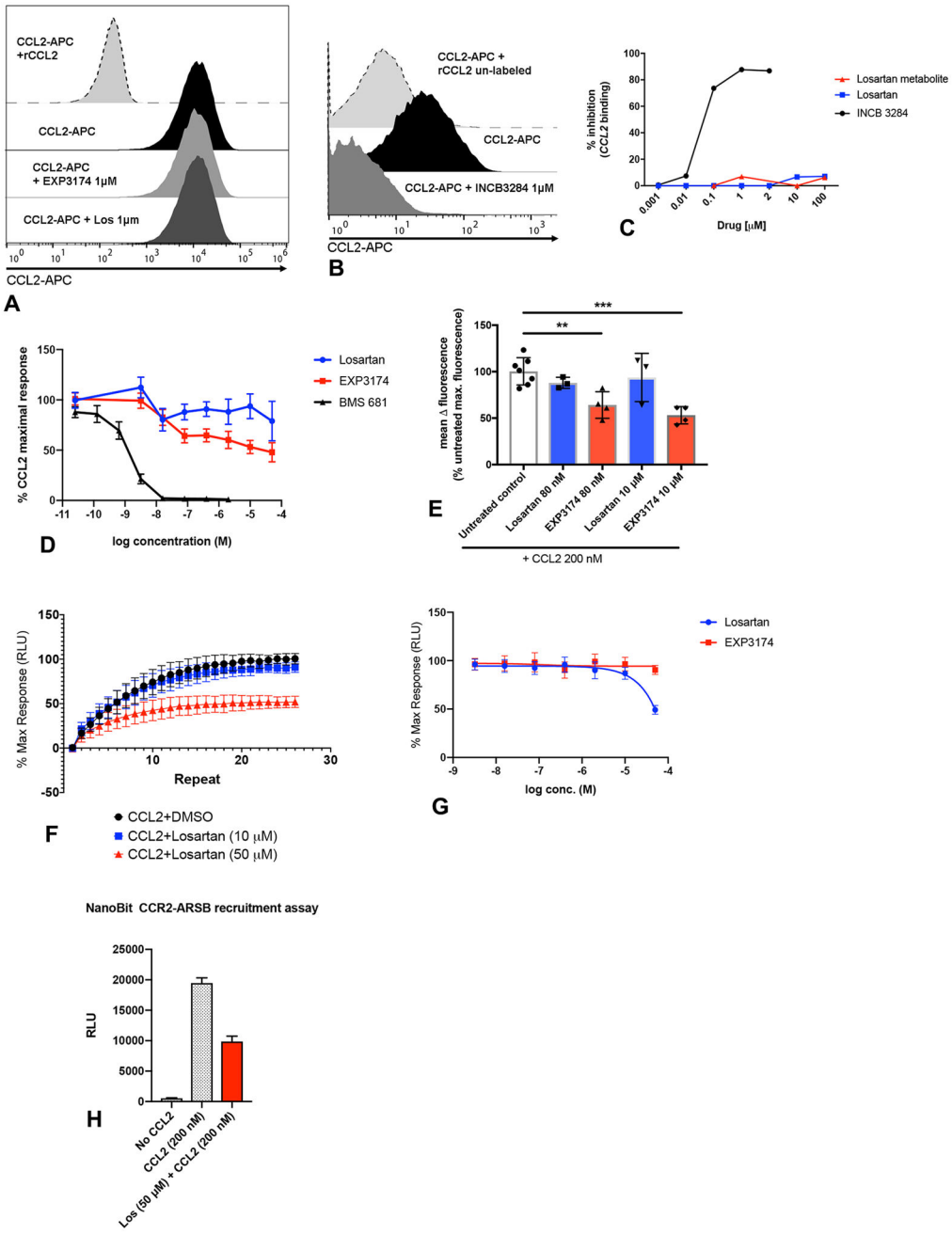

Figure 2.

Losartan and its EXP3174 metabolite do not block *CCL2* binding or *CCL2*-induced cytoplasmic Ca^{2+} release in THP-1 monocytes. **(A-C)** *CCL2* binding was assessed by flow cytometry using fluorescently labeled human r*CCL2* (CCL2-APC). **(A)** Representative histograms showing complete lack of inhibition of *CCL2* ligand binding by losartan or EXP3174 metabolite, which is in striking contrast to the orthosteric *CCR2* antagonist, INCB3344 shown in **B**. **(C)** Dose-response curve of % inhibition of *CCL2* binding for losartan, EXP3174 metabolite, and INCB3344, as determined by flow cytometry, across a range of drug concentrations. **(D)** Dose-response curve of calcium mobilization in CCR2-

expressing HEK293 cells in response to 200 nM *CCL2* +/− 1hr pre-treatment with the indicated concentrations of losartan, EXP3174, or the orthosteric *CCR2* antagonist BMS681. Cells were loaded with FLIPR calcium-sensitive dye to detect *CCL2*-induced calcium flux over time using the kinetics measurement function of a fluorescent plate reader. **(E)** Quantitative bar graph of inhibition of *CCL2*-stimulated calcium mobilization by losartan and EXP-3174, as % of untreated positive control cells. **p < 0.01, ***p < 0.001, one-way ANOVA. Data representative of the means of 3–4 independent experiments, each performed in triplicate. **(F)** 30-min kinetic read, and **(G)** dose-response curve, of β-arrestin recruitment to CCR2 in HEK293 cells in response to 200 nM *CCL2* +/− pre-treatment with the indicated concentrations of losartan or EXP3174. Cells were transfected with a NanoBiT CCR2-ARRB1 luciferase construct to monitor *CCL2*-induced CCR2-β-arrestin interaction over time using the kinetics measurement function of a luminometer. Data representative of the mean of 3 independent experiments each performed in triplicate. **(H)** Quantitative bar graph of end-point luminescence values of the CCR2-β-arrestin recruitment kinetic curve shown in (F). Data represents one of three independent experiments each performed in triplicate. Error bars, SEM (**D**) or SD (**E, F, G, H**).

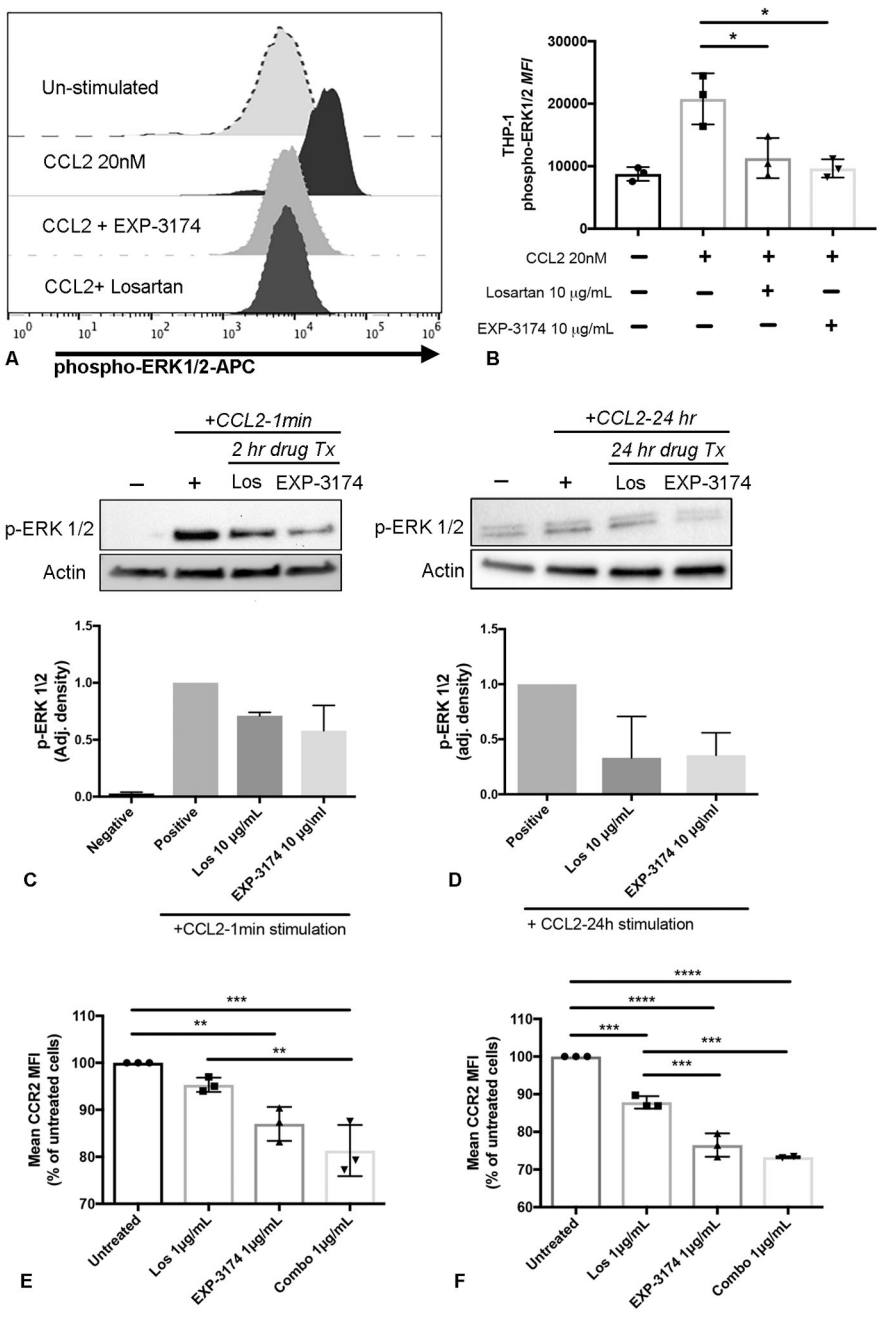

Figure 3.

Losartan and its EXP3174 metabolite inhibit *CCL2*-mediated *ERK 1/2* phosphorylation and decrease cell surface CCR2 expression in THP-1 monocytes. **(A)** Histograms showing flow cytometric detection of phospho-*ERK 1/2* in naïve, un-stimulated THP-1 cells, or THP-1 cells stimulated for 3 min with 20nM *CCL2*, +/− 1hr pre-treatment with losartan orEXP3174 metabolite at 10 μg/mL. **(B)** Quantification of Phospho-ERK1/2 mean fluorescence intensity in THP-1 cells shown in **A**. *p < 0.05, one-way ANOVA, *n* = means of 3 independent experiments performed in duplicate or triplicate. **(C and D)** Western blot images and quantitative bar graphs of the effects of losartan and EXP3174 metabolite treatment on

inhibition of *ERK1/2* activation in THP-1 cells following acute **(C)** or prolonged **(D)** *CCL2* agonist stimulation. For both **C** and **D**, *n* = means of 2 independent experiments for each time point. **(E** and **F)** Quantitative bar graphs of cell surface CCR2 expression assessed by flow cytometry in THP-1 cells following 4 h (**E**) and 24 h (**F**) drug treatment at clinically relevant concentrations. For both (E) and (F), **p < 0.01, ***p < 0.001, ****p<0.0001, one-way ANOVA, *n* = means of 3 independent experiments performed in triplicate. Error bars, SD.

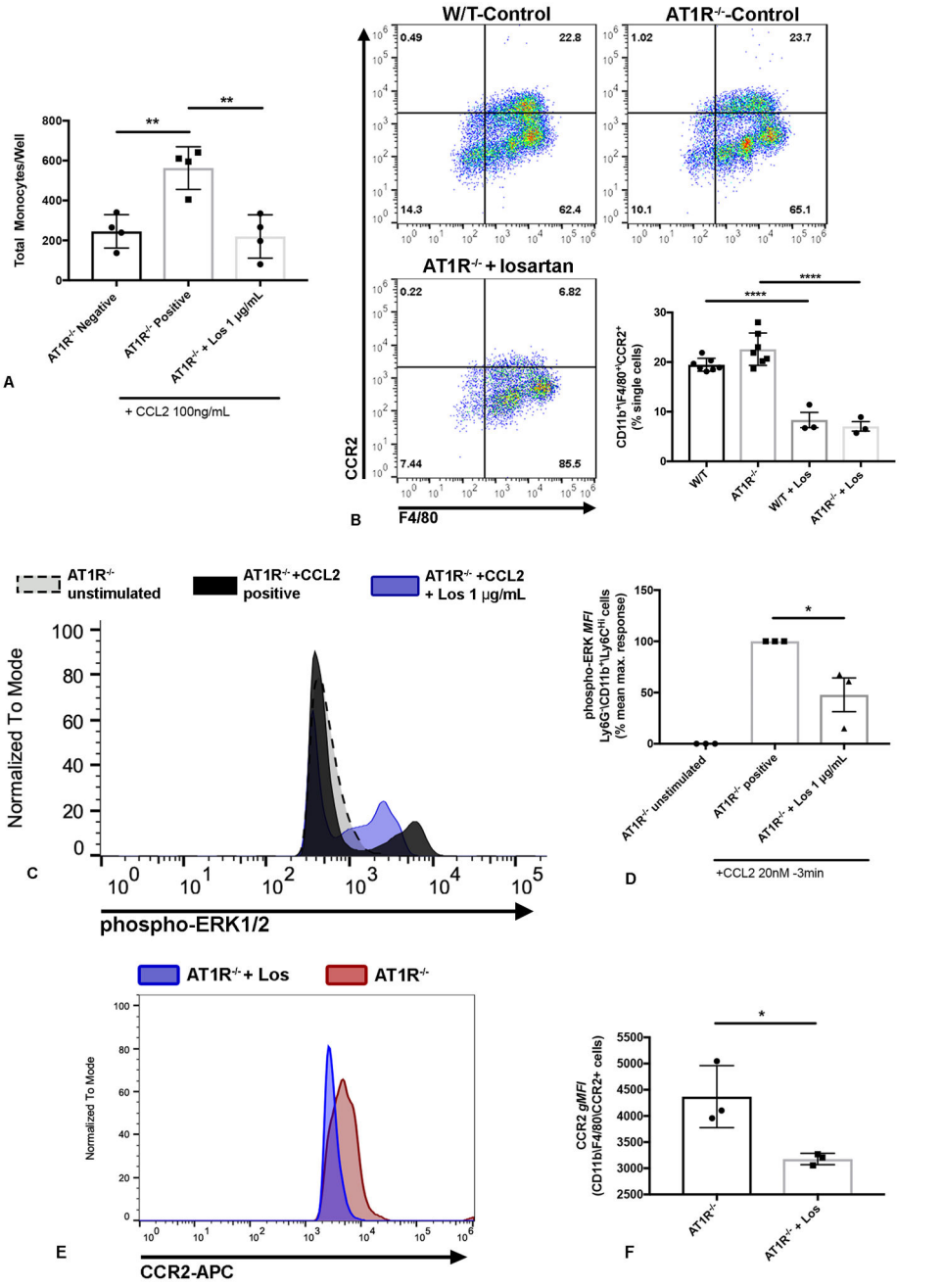

Figure 4.

Losartan-mediated blockade of CCL2-CCR2 signaling and monocyte recruitment does not require the presence of its biological target *AT1R*. **(A)** Graph of quantification of in vitro trans-well migration assay demonstrating the ability of losartan to inhibit *CCL2*-mediated migration of AT1R KO bone marrow cells. **p < 0.01, one-way ANOVA, $n = 4$ replicates from two independent experiments, each the sum of (16) 10x magnification fields/replicate. **(B)** Representative flow plots and quantitative bar graph of % *CD11b*$^{+}$/*F4/80*$^{+}$/*CCR2*$^{+}$ monocytes in peritoneal lavage fluid collected 72h post i.p. injection of thioglycollate in wild-type C57BL/6J mice *(top left)*, AT1R$^{-/-}$ mice (top right), or AT1R$^{-/-}$ mice treated with

losartan 60mg/kg/day *(bottom right)*. ****p < 0.0001, *n* =3–7 mice per group from two independent experiments. **(C)** Histogram overlay showing flow cytometric detection of *ERK 1/2* phosphorylation in un-stimulated, CCL2-stimulated (20nM, 3 min), or losartan pre-treated and CCL2-stimulated *CD11b*$^{+}$*/Ly6C*^{Hi} bone marrow monocytes collected from AT1R KO mice. **(D)** Quantitative bar graph of phospho-ERK1/2 mean fluorescence intensity in AT1R KO monocytes shown in **C**. The maximum *CCL2*-induced phospho-ERK response was determined as the mean difference in p-*ERK1/2* mean fluorescence intensity (MFI) between unstimulated and *CCL2*-stimulated monocytes. *p < 0.05, one-way ANOVA, *n* = 3 per group, each the mean of duplicates or triplicates. **(E)** Histogram overlay of CCR2 expression in CD11b^{+}/F4/80^{+} peritoneal macrophages collected, 72h post-thioglycollate injection, from untreated (red) or losartan-treated (blue) AT1R KO mice. **(F)** Quantitative bar graph of CCR2 geometric mean fluorescence intensity (gMFI) in AT1R KO peritoneal macrophages shown in **E**. *p < 0.05, *t* test, *n* = 3 per group, from one representative of two independent experiments. Error bars, SEM.

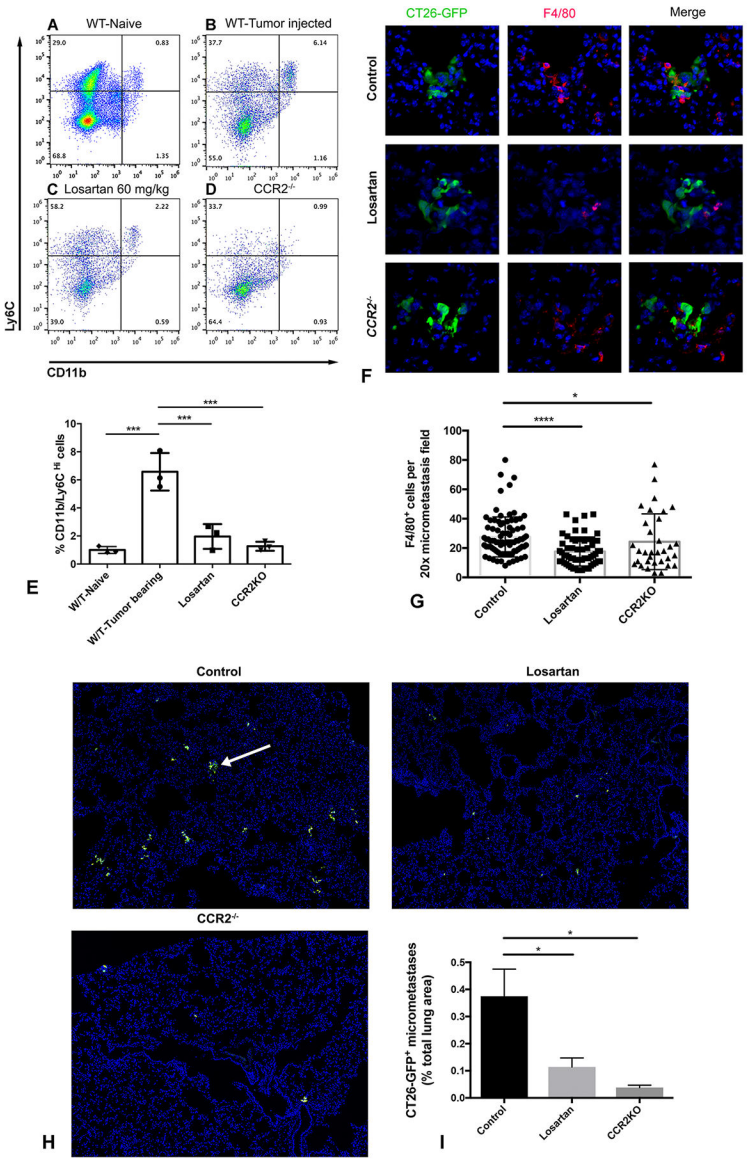

Figure 5.

Losartan blocks tumor-mediated inflammatory monocyte recruitment to the lungs and reduces the establishment of early CT26 pulmonary micrometastases. **(A-D)** Representative flow plots of *CD11b*$^{+}$*/Ly6C*^{Hi} IMs in the lungs of either naïve Balb/c mice **(A)**, or 72 hours post tail-vein injection of CT26-GFP tumor cells (4×10^5 cells) in control mice **(B)**, mice treated with Losartan 60mg/kg **(C)**, or *CCR2*$^{-/-}$ mice **(D)**. **(E)** Quantitative bar graph of inflammatory monocytes, as detected by flow cytometry in the lungs of the groups of mice shown in **A-D**. ***p < 0.001, one-way ANOVA, $n = 3$ per group. **(F)** Corresponding immunofluorescent images of lung cryosections demonstrating F4/80^{+} metastasis-associated macrophages (MAMs, red) surrounding CT26-GFP+ micrometastases (green) in control, losartan-treated, and *CCR2*$^{-/-}$ mice. **(G)** Quantitative bar graph of F4/80+ MAM density, as detected by immunofluorescent microscopy, in the lungs of the groups of mice in **F**. ****p < 0.0001, *p < 0.05, one-way ANOVA, $n = 3$ per group, 10–46 micrometastases analyzed per

mouse. **(H)** Representative 20x magnification immunofluorescent images of lung cryosections of mice from experimental metastasis assays demonstrating the density of CT26-GFP^{+} tumor cell clusters (green, white arrow) in control (*top left*), losartan treated (*top right*), and *CCR2*$^{-/-}$ mice (*bottom left*). **(I)** Graph depicting quantification of micrometastatic burden (CT26-GFP+ tumor cell area as % of total lung area) for groups of mice shown in **H**. *$p < 0.05$, one-way ANOVA, $n = 3$ per group. Error bars, SD.

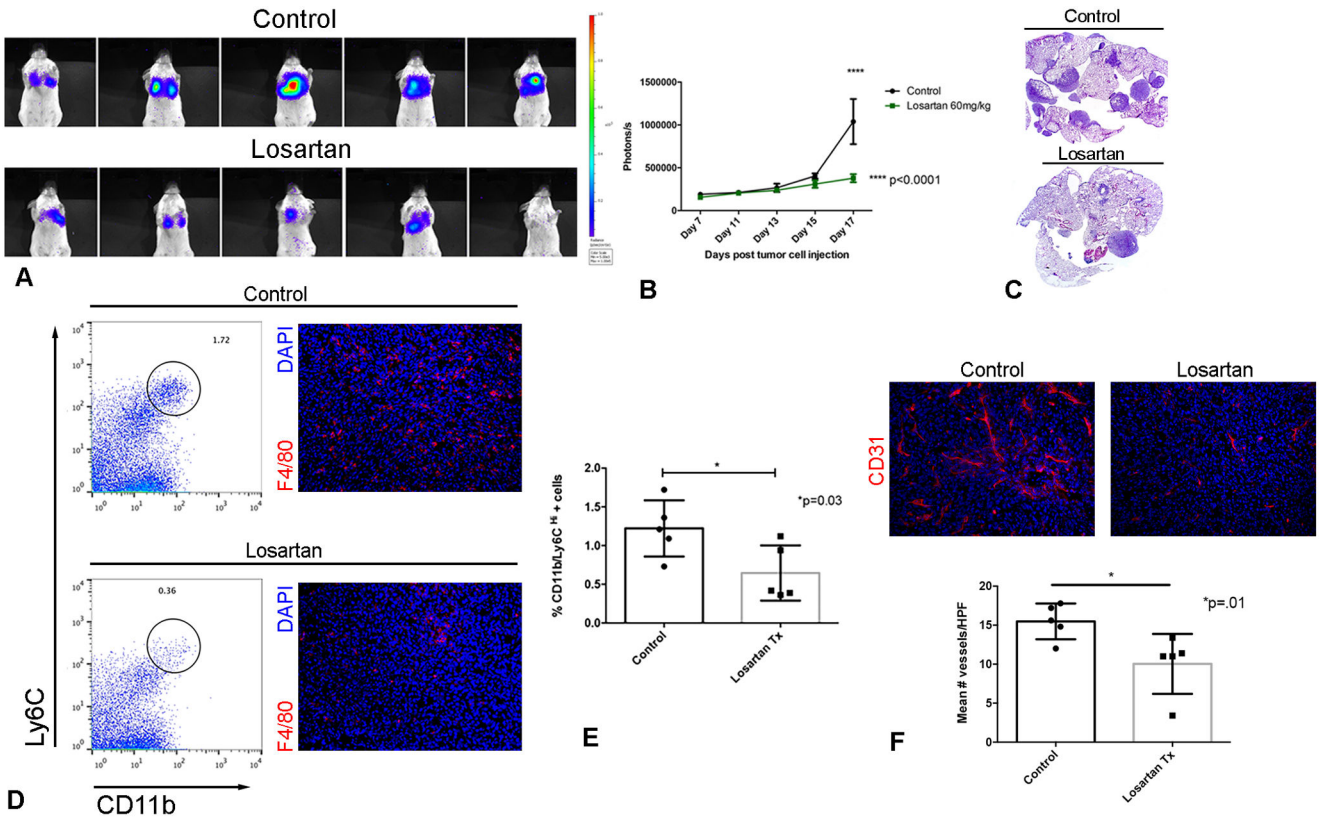

Figure 6.

Daily treatment with losartan is associated with sustained blockade of monocyte recruitment and reduced pulmonary metastasis growth in a CT26luc experimental metastasis model**. (A)** IVIS bioluminescent images of CT26luc pulmonary metastases in control and losartan-treated mice on day 17, immediately prior to euthanasia. **(B)** Quantification of CT26luc pulmonary metastatic burden over time by repeated bioluminescent IVIS imaging. ****p < 0.0001, two-way ANOVA, $n = 5$ per group. **(C)** Representative sub-gross micrographs of the lungs of mice from control and losartan treated groups shown in **A&B**. **(D)** Representative flow plots of $CD11b^{+}/Ly6C^{Hi}$ lung monocytes, and corresponding $F4/80^{+}$ immunofluorescent images of cryosections of pulmonary metastases. **(E)** Bar graph of flow cytometric quantification of lung inflammatory monocytes at sacrifice for the groups of mice shown in **A-D**. *p = 0.03, *t* test, $n = 5$ per group. **(F)** Representative immunofluorescent images and quantitative bar graph of $CD31^{+}$ micro-vessel density of cryosections of CT26 pulmonary metastases. *p = 0.01, *t* test, $n = 5$ per group. Data are from one representative of two independent experiments. Error bars, SD

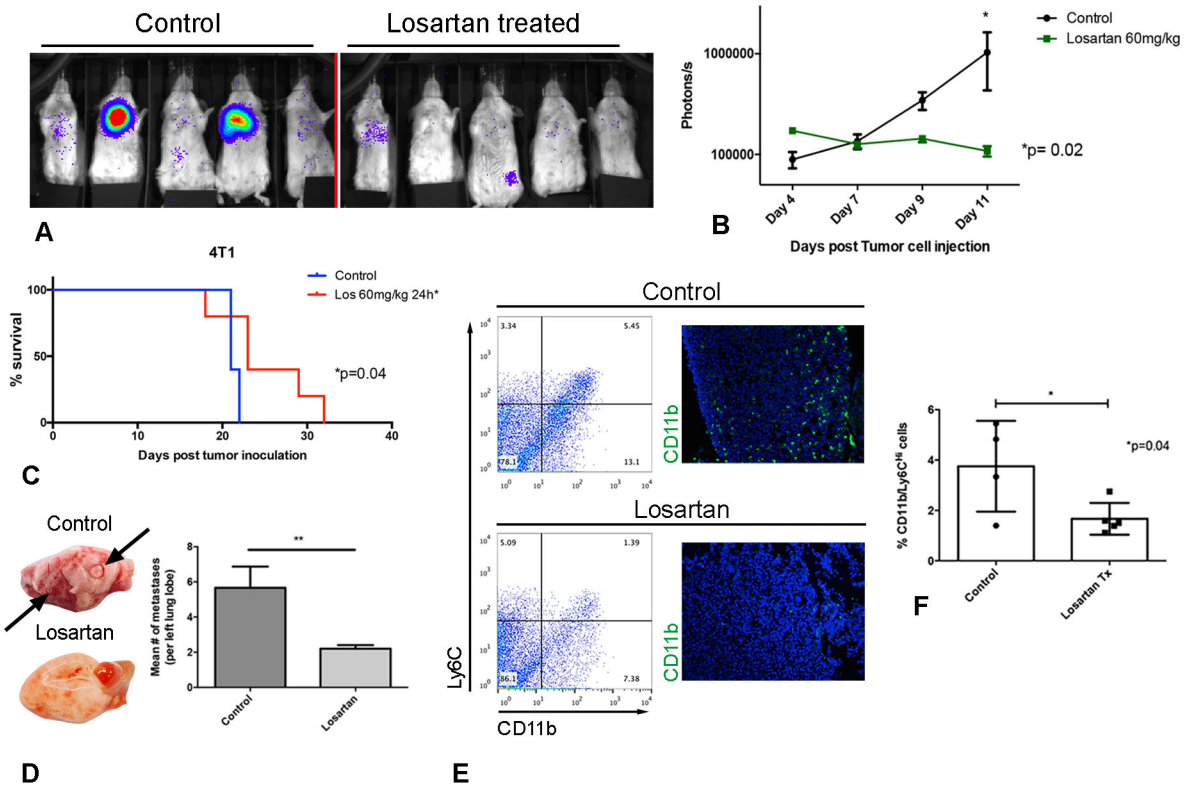

Figure 7.

Losartan demonstrates anti-metastatic activity associated with blockade of monocyte recruitment in a 4T1luc experimental pulmonary metastasis model**. (A)** IVIS bioluminescent images of 4T1luc pulmonary metastases in control and losartan-treated mice on day 11, immediately prior to euthanasia. **(B)** Quantification of the 4T1luc pulmonary metastatic burden over time by repeated bioluminescent imaging. *p = 0.02, two-way ANOVA, $n = 5$ mice per group. **(C)** Kaplan-Meier (KM) survival curves of 4T1luc control or losartan-treated mice. *p = 0.04, Log-rank test, $n = 5$ per group in two independent experiments. **(D)** Histological quantification of pulmonary metastatic burden as assessed by H&E staining of lungs from mice in **A**. ***p < 0.01, t test*, $n = 5$ mice per group. **(E)** Representative flow plots of $CD11b^{+}/Ly6C^{Hi}$ lung monocytes, and corresponding $CD11b^{+}$ immunofluorescent images of pulmonary metastases. **(F)** Bar graph of flow cytometric quantification of lung IMs at sacrifice for the groups of mice shown in **A** and **B**. * p = 0.04, *t* test, $n = 4–5$ mice per group. Data are from one representative of two independent experiments. Error bars, SD.